Chemosphere. Volume 300, August 2022, 134623. PREPRINT (submitted version)
https://www.sciencedirect.com/science/article/pii/S004565352201116X?via%3Dihub
https://doi.org/10.1016/j.chemosphere.2022.134623

Photocatalytic activity of CuO nanoparticles for organic and inorganic pollutants removal in wastewater remediation

Assefu Kassegn Sibhatu [a], Getu Kassegn Weldegebrieal [b*] , Suresh Sagadevan [c*], Nam Nghiep Tran[d] and Volker Hessel[d*]

[a]Department of Physics, College of Natural and Computational Sciences, Debre Berhan University, Ethiopia

[b]Department Chemistry, College of Natural and Computational Sciences, Debre Berhan University, Ethiopia

[c]Nanotechnology & Catalysis Research Centre, University of Malaya, Kuala Lumpur 50603, Malaysia

[d]School of Chemical Engineering and Advanced Materials, The University of Adelaide, North Terrace Campus, Adelaide 5005, Australia

[*] Corresponding author e-mail: belay.kassegn@gmail.com; drsureshnano@gmail.com; volker.hessel@adelaide.edu.au

Abstract

Heterogeneous photocatalysis is a promising technology for eradicating organic, inorganic, and microbial pollutants in water and wastewater remediation. It is the more preferable method to other conventional wastewater treatment approaches on account of its low cost, environmental benignity, ability to proceed at ambient temperature and pressure conditions, and its capability to completely degrade pollutants under appropriate conditions into environmentally safe products. Copper (II) oxide or cupric oxide (CuO) is an intrinsically p-type transition metal oxide semiconductor with a narrow bulk band gap of 1.2 eV at room temperature (RT). It is multifunctional oxide and especially its application in photocatalytic removal of contaminants

from aqueous media has attracted researchers' interest mainly because of its chemical stability and sensitivity in the visible region of the electromagnetic spectrum. However, rapid charge carrier recombination and their slow kinetics are the principal bottlenecks that severely affect its efficiency as a photocatalyst and researchers have mitigated these problems by employing several approaches including modifying its particle morphology, doping with elements, coupling with other semiconductors or utilizing diverse supporting substances. This review provides an overview of these strategies as well as the impact of different operational parameters on the removal proficiency of various organic and inorganic pollutants in water and wastewater treatment based on the latest reports in the literature.

Keywords: Cupric oxide, Heterogeneous photocatalysis, Organic pollutants, Toxic heavy metal ions, Wastewater remediation

1. Introduction

Clean and safe water is a vital commodity for humans' survival. It is used in multiple applications including for drinking, food preparation, running businesses, and irrigation purpose. Though about 71% of the surface of the Earth is covered with water, only nearly 3% of it is freshly available locked up in the form of glaciers and ice and of which a very minute fraction is available in liquid form on the surface in rivers, lakes and the atmosphere [1]. This fresh water could potentially be contaminated with natural or primarily anthropogenic activities. Wastewater may be defined as water that has been used or is affected in quality due to the presence of foreign potential contaminants, making it inconvenient for many applications and it could emerge from different sources including households, industrial sites, and agricultural sites.

Wastewater could be the cause for the transmission of diverse water-borne diseases such as typhoid, cholera, diarrhea, dysentery, polio, etc. in humans [2]. Wastewater treatment is any activity carried out to remove these foreign substances from it and is a crucial step to avoid the shortage of clean and safe water and ensure its sustainable utilization. The treatment methods can generally be classified as physical, chemical, biological or a hybrid of these. In the physical method, physical pollutants of wastewater such as suspended solid particles and floating oil or foam are removed by settling and skimming from the top surface, respectively. Chemical treatment includes the deliberate addition of chemicals to act as flocculants to promote precipitation of dissolved substances or as disinfecting agents such as chlorine, ozone or chlorine dioxide to neutralize microorganisms. Whereas, biological treatment method depends on the utilization of microorganisms to breakdown organic pollutants from wastewater through normal cellular processes. Conventional wastewater treatment approaches include adsorption on activated carbons, chemical oxidation and reduction, chemical precipitation, flocculation, flotation, and so forth. These are costly and do not involve the destruction of pollutant substances and have inefficient removal efficiency [3]. Due to the complex nature of the wastewater matrix, adequate decontamination of wastewater is difficult to achieve and in practice, a combination of the mentioned methods is employed to get quality water more economically [4].

Advanced oxidation processes (AOPs) are wastewater treatment methods in which the pollutants are removed by redox reactions of in situ generated hydroxyl radicals. Such systems include the addition of ozone (O_3), UV/O_3, UV/H_2O_2, UV/O_3/H_2O_2, Fe^{2+}/H_2O_2 (Fenton's reagent), etc. The advantages of these systems include fast reaction kinetics, small footprint in the treated water, no formation of sludge and hence reduced cost of treatment, can proceed at mild temperature

and pressure conditions, can completely degrade pollutants under appropriate conditions, are simpler to operate, and are easily integrable with other treatment approaches [5, 6]. However, the high cost of chemical utilization needed to maintain the operation of the system is one of their main shortcomings.

Once generated, these reactive radicals can decompose not only organic pollutants initially into intermediate species and finally into CO_2, H_2O, and few mineral acids [7] but also they can neutralize microorganisms as well as remove toxic heavy metal ions such as Cr (VI), Ag (I), Pb (II), and Hg (II) from water and wastewater via oxidation or reduction reactions. Thus, heterogeneous photocatalysis may be used in wastewater reclamation by removing its organic, inorganic, and biological contaminants and goes through five independent steps during the process [8]. At the heart of heterogeneous photocatalytic reactions is the semiconductor catalyst. Though there are different types of semiconductor catalysts that have been used such as transition metal sulfides, chlorides, and phosphides and non-metallic organic semiconductors such as graphene oxide (GO), graphitic carbon nitride (g-C_3N_4) or a hybrid of one or more of them, transition metal oxides are interesting photocatalysts because of their easier synthesis and ability to form different metal-oxygen ratios, due to their half-filled d orbitals that enable them to form different oxidation states, with varying properties and catalytic pollutants removal performance [9].

Copper (II) oxide or cupric oxide (CuO) is a transition metal oxide having numerous applications in different fields. It is an intrinsically p-type semiconductor oxide owing to oxygen vacancy defects in its crystal structure and has an indirect narrow bulk bandgap of 1.2 eV at RT [10]. It has monoclinic crystal structure with space group C2/c and lattice constants of a = 4.6837, b = 3.4226, c = 5.1288 Å, and β = 99.54° [11]. Copper (I) oxide or cuprous oxide (Cu_2O) and

copper (III) oxide (Cu_4O_3) are other polymorphs and while Cu_2O is a thermally less stable phase than CuO, Cu_4O_3 is a metastable phase with a mixed oxidation state of Cu atom and is difficult to synthesize [12, 13]. CuO appears in brownish-black powder and is used in many applications including in magnetic storage media, high-temperature superconductors, as an electrode in dye-sensitized solar cells, lithium-ion batteries, and solid oxide fuel cells, in chemical and gas sensors, catalysis, pharmacy in antitumor therapy, as an antimicrobial agent in food preservation, biomedicine to prevent bacterial infection of biomedical devices, textile to produce antibacterial textile fabrics, and in photocatalysis to decompose organic pollutants from water or wastewater [14-20].

This review emphasizes the photocatalytic activity response of CuO nanostructures for the removal of organic and inorganic pollutants in aqueous media based on the latest reports in the literature. In doing so, removal mechanism, factors influencing the efficiency of decontamination of the pollutants, and ways of mitigating the bottlenecks for effective removal are overviewed in detail and finally ends with a recap of the main points discussed.

2. Photocatalytic activity of CuO nanoparticles

Wastewater may bear physical, chemical and biological impurities of which organic and inorganic pollutants discharged from various sources are very common. CuO nanostructures are one among many interesting photocatalysts utilized by researchers for the elimination of these pollutants under their abundance, low cost, narrower bandgap, excellent chemical stability, and facile synthesis [21]. Before discussing the photocatalytic activity of CuO NPs, the nature and types of some of the toxic organic and inorganic pollutants in aqueous media are highlighted first.

2.1 Toxic organic and inorganic pollutants

Water pollutants of organic or inorganic nature are common and complex depending on their source of origin. In particular organic pollutants are extremely varied in type and composition depending on their source. While those pollutants discharged as effluents from single factories are named point sources those that emerge from multiple sources such as agricultural run-off, storm drainages, and construction sites are non-point sources. These pollutants could affect human health by causing diseases or harming skin surfaces, disturb aquatic life via creating oxygen deficiency and make waterbodies unpleasant to use or destroy the natural aesthetic beauty or health of the water bodies. Pollutants may be classified into different types in terms of whether their consequences are known and there is already developed an analytical method of monitoring them. These include priority pollutants, emerging pollutants, and persistent organic pollutants. Priority pollutants are types of pollutants where their toxicity to humans and the environment is well established and for which there is already developed a method of analyzing and monitoring them. Whereas, emerging pollutants are those types of pollutants whose effect on humans, animals, and the environment is not known because they are either newly synthesized or they are already there but no toxicity data is available about them. Persistent organic pollutants are contaminants having the capability to resist chemical, biological, and photochemical degradation and have the ability to stay longer without being decomposed, and can reach toxic concentration levels starting from smaller exposure owing to their capability to bioaccumulate, biomagnify via the food chain, and can transfer long-range distances by evaporation and precipitation methods [22]. As a consequence, these compounds are risky to humans' health and are regulated under the Stockholm convention adopted in 2001 which is effective as of 2004 [23].

Endocrine disruptors are compounds that interfere with humans and wildlife hormones and can cause various reproductive and neurological health problems [24]. Endocrine-disrupting organic compounds include pesticides such as DDT, methoxychlor, atrazine and those used in making plastics and food storage materials such as phenol, bisphenol A, and phthalates and also other industrial compounds such as polychlorinated biphenyls (PCB) and dioxins [25]. On the other hand, neurotoxins are substances that interfere with the normal functioning of the nervous system including carbon disulfide, n-hexane, toluene, etc [26]. Mutagens are substances that induce DNA mutation or damage and teratogens are also compounds that cause malformations in embryos both of which result in birth defects. Carcinogenic substances cause various cancerous tumors in the body.

Inorganic pollutants in wastewater including substances such as halides, heavy metals, oxyanions and cations, radioactive materials, etc are a threat to humans health and the environment on account of their recalcitrance to biodegradation and photocatalytic decomposition and hence their capability to persist long in aqueous systems [27]. The toxicity of various organic and inorganic substances is overviewed in references [28, 29] and specific examples of toxic heavy metal ions. It is, therefore, essential to properly treat wastewater before being discharged into the environment and potentially cause harmful consequences to the environment, humans as well as aquatic biota.

2.2 Photocatalytic activity of CuO NPs for organic pollutants

Being a semiconductor with a narrow bandgap, CuO is active in the visible wavelength region of the electromagnetic spectrum. The conspicuous advantage of this is that nature sunlight whose predominant radiation reaching the surface of the earth is visible may be used to stimulate the

photocatalytic decomposition process of organic pollutants; however, the drawback associated with it is the high probability of photogenerated e^-/h^+ pairs recombination which suppresses the photonic and hence removal efficiency. As a consequence, improving some of its surface morphological properties via improved synthetic route and optimizing experimental parameters are crucial to maximize the degree of decomposition of organic contaminants in water and wastewater reclamation using CuO NPs as photocatalysts.

2.2.1 Mechanism of photocatalytic decomposition of organic pollutants

Photocatalytic decomposition of organic pollutants using semiconductor photocatalysts may occur through direct or indirect mechanistic routes. In the direct mechanism, the hydroxyl radical ($HO^{\cdot}$) and superoxide radical ion ($O_2^{-\cdot}$), the two reactive radicals mainly responsible for the degradation of pollutants, are generated in the reaction system by the direct injection of photoexcited electrons from the pollutant organic molecules (OM^*) into the CB of the semiconductor, where it gets itself oxidized to give radical cation ($OM^{+\cdot}$) and reduces dissolved O_2 to $O_2^{-\cdot}$, Eq. (8-9) and then to $HO^{\cdot}$ via a sequence of steps as shown in Eq. (5-7) and graphically illustrated in Fig.1.

$$CuO + h\nu \rightarrow CuO\ (e^- + h^+) \quad (1)$$

$$O_2 + e^- \rightarrow O_2^{-\cdot} \quad (2)$$

$$H_2O + h^+ \rightarrow HO^{\cdot} + H^+ \quad (3)$$

$$HO^- + h^+ \rightarrow HO^{\cdot} \quad (4)$$

$$O_2^{-\cdot} + H^+ \rightarrow HOO^{\cdot} \quad (5)$$

$$2HOO^{\cdot} \rightarrow H_2O_2 + O_2 \quad (6)$$

$$H_2O_2 \rightarrow 2HO^{\cdot} \quad (7)$$

$$OM + h\nu \rightarrow OM^* \quad (8)$$

$$OM^{*} + O_2 \rightarrow O_2^{-\cdot} + OM^{+\cdot} \quad (9)$$

$$OM + OM^{+\cdot} + HO^{\cdot}/O_2^{-\cdot} \rightarrow \text{Decomposed products} \quad (10)$$

However, in the indirect route, Fig.1, first electron-hole (e^-/h^+) pairs are formed when electromagnetic radiation of energy (hν) greater than or equal to the bandgap energy (E_g) of the semiconductor catalyst (CuO) irradiates it and excites electrons from the valence band (VB) to the conduction band (CB), leaving holes behind in the VB. Then, these e^-/h^+ pairs may recombine giving off the excess energy in the form of heat or radiation or undergo separate redox reactions by diffusing onto the surface and reacting with nearby surface adsorbed species. That is, the photoexcited electrons reduce adsorbed O_2 to $O_2^{-\cdot}$ while the holes oxidize H_2O or HO^- to $HO^{\cdot}$, Eq. (1-4). Any strategy that minimizes the recombination and maximizes the separation of the photoproduced charge carriers results in an augmented rate of degradation. It has been found that the indirect mechanism is kinetically faster and the predominant route in the photocatalytic degradation of organic pollutants [30]. The oxidation reactions of VB holes and reduction reactions of CB electrons with catalyst surfaces adsorbed species are essential in achieving the separation of photogenerated charge carriers and promoting the rate of pollutants removal. The electron transfer mechanism and efficiency of charge carriers' separation could be different from catalyst to catalyst depending on the size of the bandgap and whether the catalyst is single phase, doped or is a mixed phase. After they are in situ produced, the reactive radicals start off attacking the pollutant compounds via hydrogen abstraction, electron transfer, radical addition and combination modes [31].

Chemosphere. Volume 300, August 2022, 134623. PREPRINT (submitted version)
https://www.sciencedirect.com/science/article/pii/S004565352201116X?via%3Dihub
https://doi.org/10.1016/j.chemosphere.2022.134623

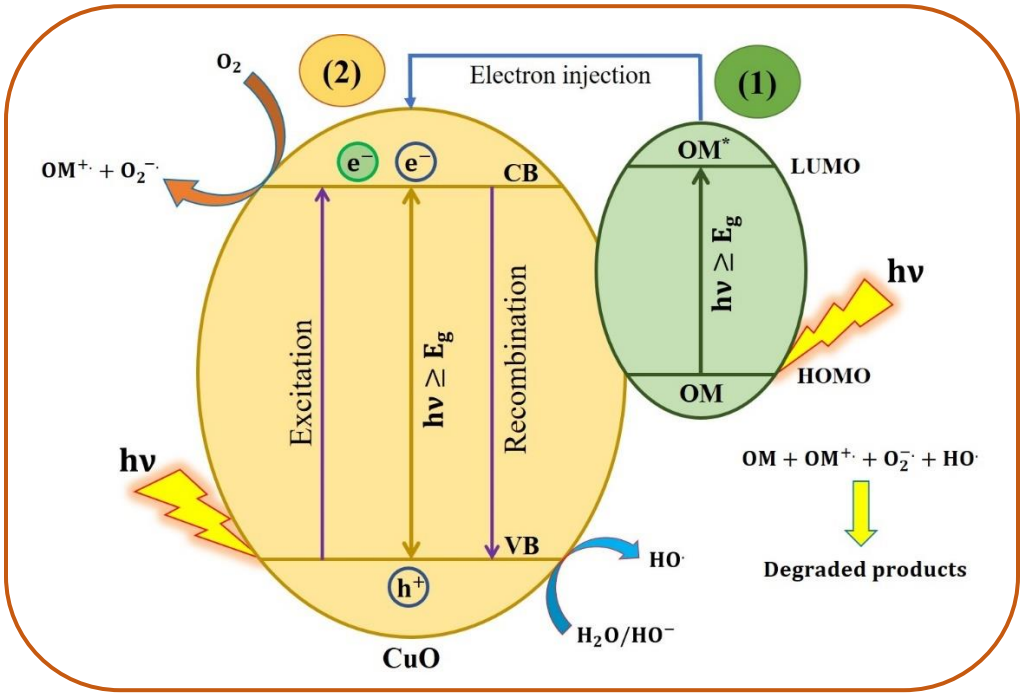

Figure 1. Illustration of general photocatalytic electron transfer and degradation reaction mechanism of organic pollutants.

Even though the exact mechanistic route leading to the eventual mineralization of organic pollutants is difficult to track due to the complex nature of the reaction, rough routes by which the destruction occurs could be proposed based on experimental evidence from, for example, GC/MS or LC/MS result of reaction mixture taken at different time intervals.

As a consequence, researchers have proposed various possible photocatalytic decomposition mechanistic pathways for different organic pollutants in water and wastewater. For instance, Bhattacharjee and Ahmaruzzaman [32] reported that during the photocatalytic degradation of methylene blue identification of the fragmentation products from the mass spectra from LCMS data showed the breakage of the dye molecules along the broken line denoted by “b” (Figure 2) in the thiazine ring to produce intermediate phenol and p-aminophenol products before undergoing further oxidation to give CO_2, H_2O and mineral acids. Whereas, fragmentation of the same

molecules during photocatalytic degradation reactions using Cu_2O photocatalysts was proposed to be along the broken line denoted by "a" based on evidence obtained from LC-MS data [33]. In another study, Rao *et al.* [34] proposed the degradation mechanism of tartrazine dye in the presence of CuO straw-sheaf-like nanostructures utilizing evidence obtained from GC/MS result, Figure 3.

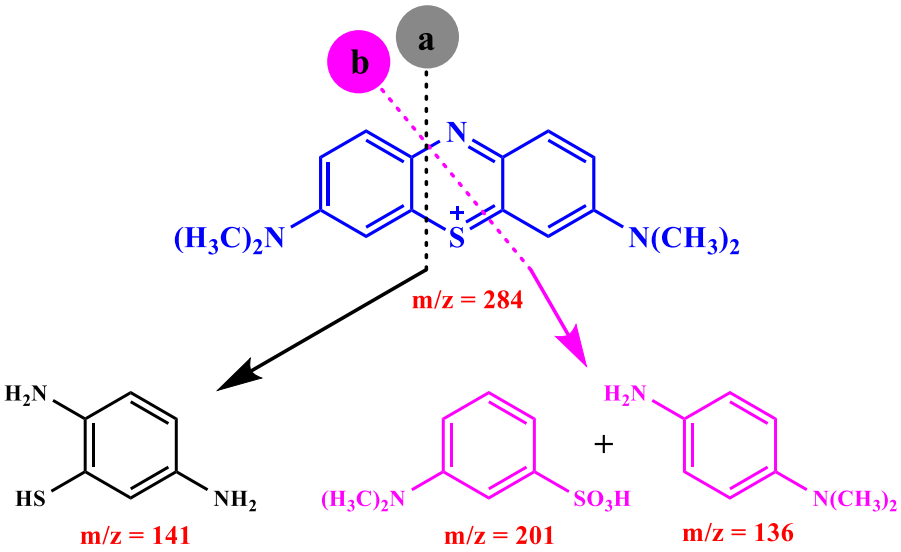

Figure 2. Fragmentation pathway of MB during photocatalytic degradation along the broken lines denoted by (a) and (b) to give the indicated intermediate products [32, 33].

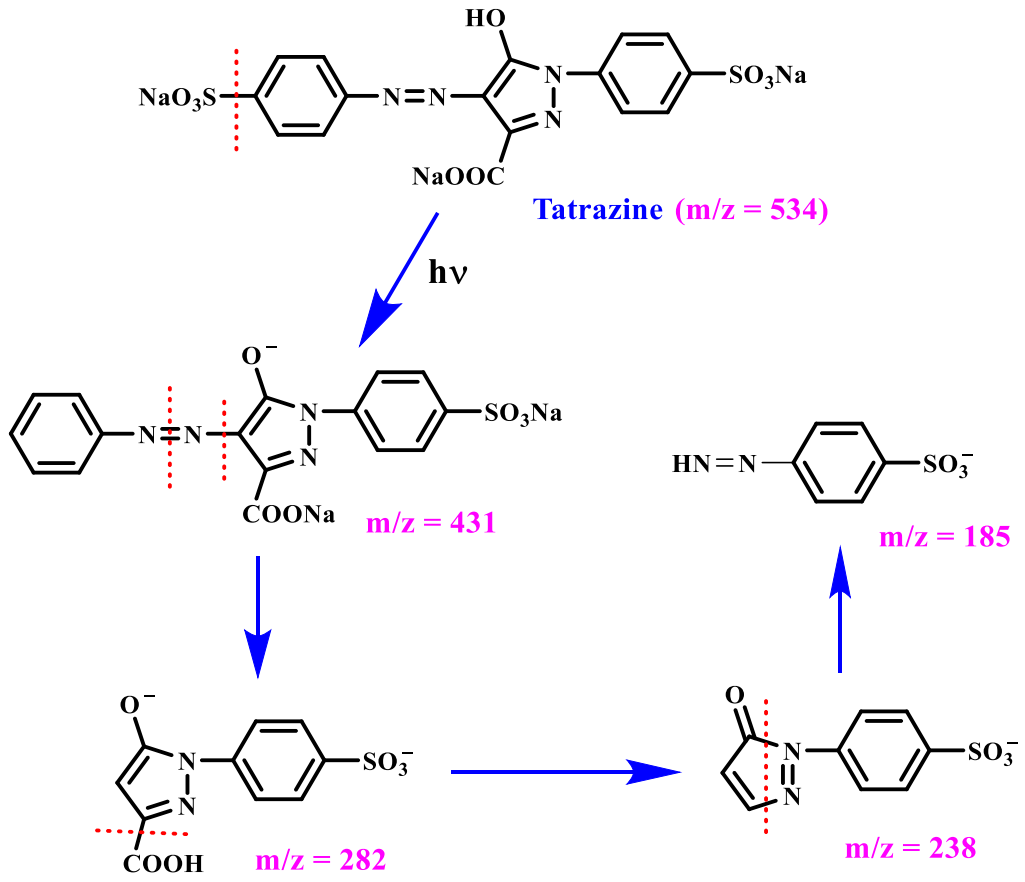

Figure 3. Proposed degradation pathway of tetrazine dye using CuO nanostructures [34].

Additionally, Raha *et al* [35] proposed the fragmentation pattern during the photocatalytic degradation of the pharmaceutical drug rabeprazole using $CuO/Mn_3O_4/ZnO$ nanocomposite as illustrated in Figure 4.

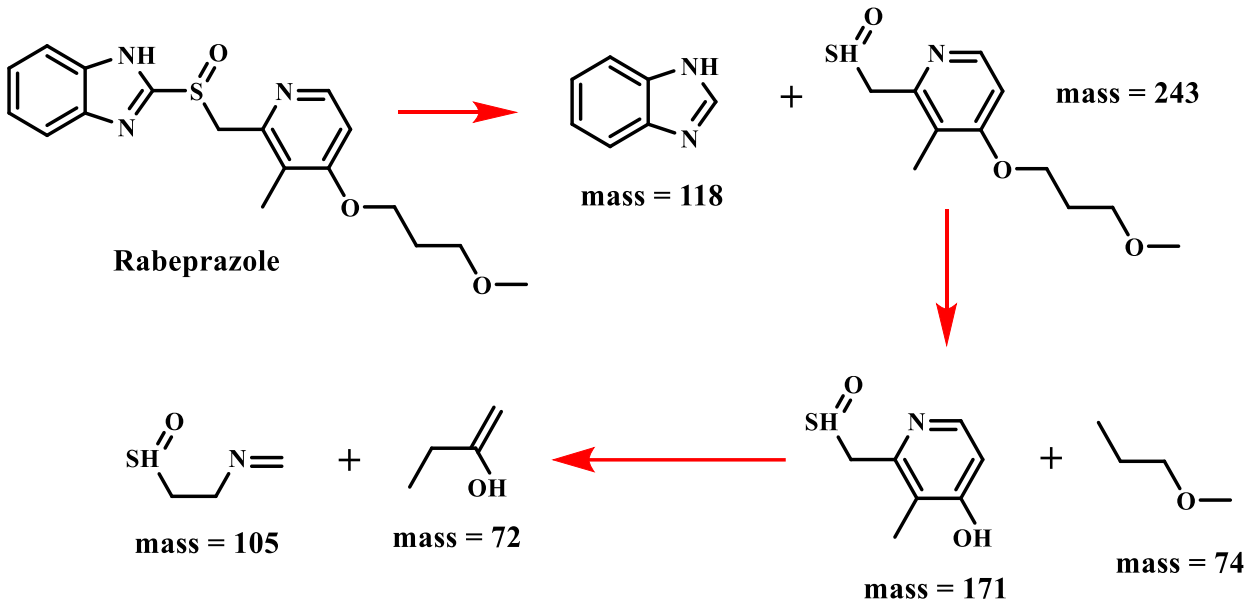

Figure 4. Proposed photocatalytic degradation mechanism of rabeprazole molecules using $CuO/Mn_3O_4/ZnO$ nanocomposite [35].

2.2.2 Test for reactive species

To test for the reactive species involved during the photocatalytic degradation process, a scavenging test is performed. In this test, reactions are carried out in the presence of scavengers for reactive species such as holes (h^+), electrons (e^-), superoxide radical ion ($O_2^{-\cdot}$), and hydroxyl radical ($HO^{\cdot}$) and information about their likely participation in the degradation process is acquired. The percentage of degradation will be retarded in the presence of scavenging species if the species have played their role in the process of decomposition reaction. For quenching $HO^{\cdot}$ radical, usually, isopropanol or t-butanol is added, and benzoquinone or ascorbic acid are employed to test for $O_2^{-\cdot}$ [36, 37]. In addition, while salts such as $NaSO_4$ or $NaNO_3$ are used for testing hydrated e^-, KI, EDTA, ammonium oxalate, etc are used for testing photogenerated h^+ [38]. So, using information obtained from the scavenging tests, the main reactive species that participated in the degradation process may be proposed. Chauhan *et al.* [39] investigated the likely involvement of $HO^{\cdot}$ during

the degradation of Victoria blue and direct red 81 dyes taken separately in the presence of CuO NPs and the scavengers of DMSO and carbonate ion. They found that the decomposition decreased in the presence of the scavengers, confirming the participation of the radicals in the degradation process. In another study reported by Haseena *et al* [40], test or reactive $HO^{\cdot}$, h^{+}, and $O_2^{-\cdot}$ species using the respective scavengers of isopropyl alcohol, triethanolamine, and p-benzoquinone, have found that removal efficiency of rhodamine B using biosynthesized CuO NPs photocatalysts decreased by 44 and 32 % in the presence of the first two respective trappers meanwhile no significant reduction was seen in the presence of $O_2^{-\cdot}$ scavenger, indicating that $HO^{\cdot}$ and h^{+} are primarily engaged in the degradation process of the dye. Whereas, inhibition of the photocatalytic decomposition of methylene blue using CuO-Cu_2O catalyst in the presence of t-butanol, ammonium oxalate, and benzoquinone added as scavengers for $HO^{\cdot}$, H^{+}, and $O_2^{-\cdot}$ indicated that all three reactive radicals have possibly participated in the degradation reaction of the dye though the inhibition was greatest in the presence of $HO^{\cdot}$ radical [41]. Further details of the types of reactive species that induced the photocatalytic degradation of organic pollutants using CuO-based photocatalysts have been recently reviewed in reference [42].

2.2.3 Kinetics of photocatalytic degradation reactions of organic pollutants

For photocatalytic degradation reactions, the photocatalyst, organic pollutant, and radiation should be in contact or proximity for the reactions to proceed and the pollutant's concentration goes decreasing with time if the employed catalyst is photoactive to the contaminant molecules under the given experimental condition. The extent of elimination or degradation (D%) of the pollutant can be obtained by observing the change in its absorbance or concentration with time using Eq. (11)

$$D\ (\%) = \frac{A_0 - A_t}{A_0} \times 100 = \frac{C_0 - C_t}{C_0} \times 100 \quad (11)$$

Where A_0, C_0, A_t, and C_t are the absorbance and concentration values initially before radiation exposure and after exposure time (t), respectively.

Regarding the kinetics of the reaction, the heterogeneous photocatalytic degradation reactions of organic pollutants mainly obey pseudo-first-order kinetics. That is the time rate of change of the concentration of the pollutant is first-order in the concentration of the pollutant and is given by Eq. (12)

$$-\frac{dC}{dt} = \kappa_1 C \quad (12)$$

Where, C is contaminant concentration and κ_1 is the pseudo-first-order reaction rate constant.

Rearranging and integrating Eq. (12) without limits gives,

$$-\int \left(\frac{dC}{C}\right) = \kappa_1 \int dt \ \Rightarrow \ln C = \ -\kappa_1 t \quad (13)$$

Integrating Eq. (12) with limits at $t = 0, C = C_0$ and at $t = t, C = C_t$ gives,

$$\ln\left(\frac{C_t}{C_0}\right) = -\kappa_1 t \Rightarrow \ln\left(\frac{C_0}{C_t}\right) = \kappa_1 t \quad (14)$$

Then, if the plot of $\ln\left(\frac{C_0}{C_t}\right)$ versus t of the experimental data give a good fit, coefficient of correlation (R^2) close enough to 1, with the generated linear regression line, then the reaction could be satisfactorily described using pseudo-first-order kinetics model. One measure of the goodness of fit between the model and experimental data is coefficient of correlation (R^2) and a value greater than or equal to 80% is suggested to be good though it alone is not enough for model validation [43]. In some cases, pseudo-second-order kinetics are also reported to have better fitted

experimental data to the model linear regression line. In pseudo-second-order kinetics, the rate of the reaction is second order in pollutant concentration, Eq. (15),

$$-\frac{dC}{dt} = -\kappa_2 C^2 \quad (15)$$

Rearranging and integrating without limits of Eq. (15) gives Eq. (16),

$$-\int \left(\frac{dC}{C^2}\right) = \kappa_2 \ dt \Rightarrow -\frac{1}{C} = \kappa_2 t \quad (16)$$

But integration in the limits at $t = 0, C = C_0$ and $t = t, C = C$, gives

$$\frac{1}{C} = -\kappa_2 t + \frac{1}{C_0} \quad (17)$$

Where, C_0 and C_t are the initial and final concentrations of the pollutant.

In a similar fashion to first-order kinetics, better fit of the experimental data to the linear regression line up on plotting $\frac{1}{C}$ versus t indicates that the reaction kinetics could be described using the pseudo-second-order model.

The relative kinetics of photocatalytic reactions can be compared with the half-life period in a similar duration of degradation reactions. The half-life of a reaction is the time it takes to reduce the initial concentration of the pollutant by half and is independent of the initial concentration of the dye used for first-order reactions, Eq. (18),

$$t_{1/2} = \frac{\ln(2)}{\kappa_1} \quad (18)$$

Where, κ_1 is the first-order reaction rate constant. The shorter the half-life, the faster the reaction and vice versa.

Unlike a pseudo-first-order reaction, the half-life of 2nd order reaction depends on the initial concentration and is given by Eq. (19),

$$t_{1/2} = -\frac{1}{C_0 \kappa_2} \quad (19)$$

Where, C_0 and κ_2 refer to the initial concentration of the organic pollutant and the second-order reaction rate constant, respectively.

2.3 Factors affecting photocatalytic degradation of organic pollutants

Photocatalytic degradation reactions are complex processes in which the elimination efficiency of organic pollutants depends on several factors. Much as other semiconductor photocatalysts, the extent of photocatalytic decomposition of the pollutants depends on such factors as morphological properties of the synthesized CuO and CuO-based catalysts, type of organic pollutant, operational parameters such as catalyst dose and pollutant initial concentration, pH, temperature, aeration and stirring rate, energy and intensity of employed radiation, and the presence of oxidants and other interferants in the reaction mixture, which are reviewed individually as under.

2.3.1 Effect of morphological properties of CuO and CuO-based catalysts on the degradation efficiency of organic pollutants

Particle size and shape could affect the rate of reactions because this affects the size of the bandgap and the diffusion length of photoproduced charge carriers from the bulk to the surface-active sites. The size of the bandgap energy in turn determines the photonic efficiency and the range of wavelengths of the electromagnetic radiation to be harvested during the degradation reactions. To maximize pollutants eradication, the bandgap should not be too small (<1.3 eV) to minimize the high probability of charge carriers recombination nor be too large (>3.0 eV) to be activated in the visible region of the electromagnetic spectrum and as such a bandgap in the range of 1.3 – 3.0 eV has generally been reported to be appropriate for photocatalytic degradation

reactions [44]. Pure CuO has a bulk bandgap of 1.2 eV and this value could reach up to 3.57 eV in the nanoscale size regime by adjusting synthesis methods [45]. However, one of its main drawbacks, when used as a photocatalyst, is the high degree of e^-/h^+ pairs recombination owing to its CB edge potential being more positive than the redox potential of hydrogen, which results in reduced catalytic activity [46]. As a consequence, its catalytic activity has been boosted via doping with other elements or coupling with other semiconductors because of the resulting enhanced features such as surface area and adsorption capacity better mobility and separation of charge carriers.

Several researchers studied the influence of particle size and shape on the degradation performance of CuO and CuO-based photocatalysts for various organic contaminants. For instance, Muthuvel *et al.* [47] found enhanced catalytic activity of CuO NPs with an average particle size of 25 nm as compared to 32 nm-sized spherical particles synthesized by chemical and biological methods, respectively towards methylene blue degradation under similar experimental conditions. In a study conducted by Junior *et al.* [48] for the degradation of the same dye using CuO NPs with different morphologies, the decomposition performance was found to increase in the order of plate-like > flower-like, boat-like > ellipsoidal like CuO particles at comparable experimental setting. Similarly, a comparison of the degradation capability of CuO nanorods, nano leaves, and nonosheets for Congo red employing the same catalyst dose of 50 mg, 100 mL of 20 ppm dye concentration under 18W UV lamp for 210 minutes showed that the particles achieved respective degradation efficiency of 67, 48, and 12% [49]. According to the authors, the observed efficiency disparity was attributed to the greater adsorption capacity arising from the higher specific surface area of the former particles than the latter. In another report by Nazim *et al.* [50],

the degradation competence of porous CuO nanosheets for the food dye Allura red AC was 97% in 6 minutes in the presence of $NaBH_4$ (1 mg/mL) under UV light irradiation and starting with 10 mL of 5 ppm dye concentration and 5 mg of CuO catalyst, which was much higher than other CuO NPs morphologies compared. This higher catalytic activity response of the CuO nanosheets to the degradation of the dye was ascribed to the greater surface area and adsorption ability of the catalyst nanosheets and also due to the augmented production of $HO^{\cdot}$ radicals via reduction of O_2 to $O_2^{-\cdot}$ and then to $HO^{\cdot}$ with electrons supplied by $BH_4^{-\cdot}$ in the reaction medium. In another study, a comparison of the photocatalytic activity of as-synthesized CuO and Tb-doped CuO for the catalytic degradation of MB for 2 hours showed that the latter improved the efficiency by 6% compared to the former [51]. This was attributed by the authors to two reasons. The first reason for the enhancement was proposed to be due to the smaller particle sizes of the Tb-doped CuO in which faster diffusion of charge carriers to the surface is facilitated, resulting in the generation of more reactive radicals and hence faster removal efficiency. The second reason is ascribed to the effective separation of photogenerated charge carriers by the presence of more surface defects which serve as electron trapping centers as well as the presence of Tb^{3+} ions on the surface of catalyst particles, acting as VB electron traps to produce Tb^{2+} and $O_2^{-\cdot}$.

One bottleneck for effective catalytic activity with narrow band gap semiconductors such as CuO is the high chance of photogenerated e^-/h^+ pairs and this has been alleviated via elemental doping or coupling it with other semiconductors. Sasikala *et al* [52] investigated the photocatalytic activity response of cerium-loaded CuO NPs for the degradation of trypan blue dye and found greater activity than pure CuO NPs. This enhancement was ascribed to the facilitated separation of photogenerated e^-/h^+ pairs due to Ce atoms serving as CB electron traps, Figure 5. Moreover,

the removal of Congo red dye with Cd, Ba-CuO was reported to be higher than Cd-CuO, Ba-CuO, and undoped CuO nanoparticles [53]. It was found that Cd, Ba-CuO degraded the dye by 98 % for 3 h degradation reaction time under visible light irradiation, an improvement by about 25% compared to undoped CuO under similar experimental settings. The higher removal efficiency of the Cd, Ba-CuO was ascribed to the inhibition of photogenerated e^-/h^+ pairs recombination by the Cd and Ba impurities forming intraband energy levels near the CB or the VB of CuO and narrowing the effective bandgap and serving as CB electron sinks, thereby promoting redox reactions to produce a large number of reactive radicals which are responsible for the destruction of dye molecules. However, elemental doping does not necessary result in an increment of activity of the metal oxides rather it could have the opposite effect. A case in point is the slight reduction observed in the degradation of methylene blue using 6% Fe-doped CuO film with degradation of 94.9 % as compared to 95.6% using CuO film for a 12 h solar irradiation as reported by Sayed and Shaban [54]. The authors suggested that the higher bandgap (2.30 eV) of 6%Fe-doped CuO film than the bandgap of pure CuO film (2.15 eV) might have caused less photons to have induced photoexcitation and formation of reactive $HO^{\cdot}$ radicals and reduced rate of degradation.

Chemosphere. Volume 300, August 2022, 134623. PREPRINT (submitted version)
https://www.sciencedirect.com/science/article/pii/S004565352201116X?via%3Dihub
https://doi.org/10.1016/j.chemosphere.2022.134623

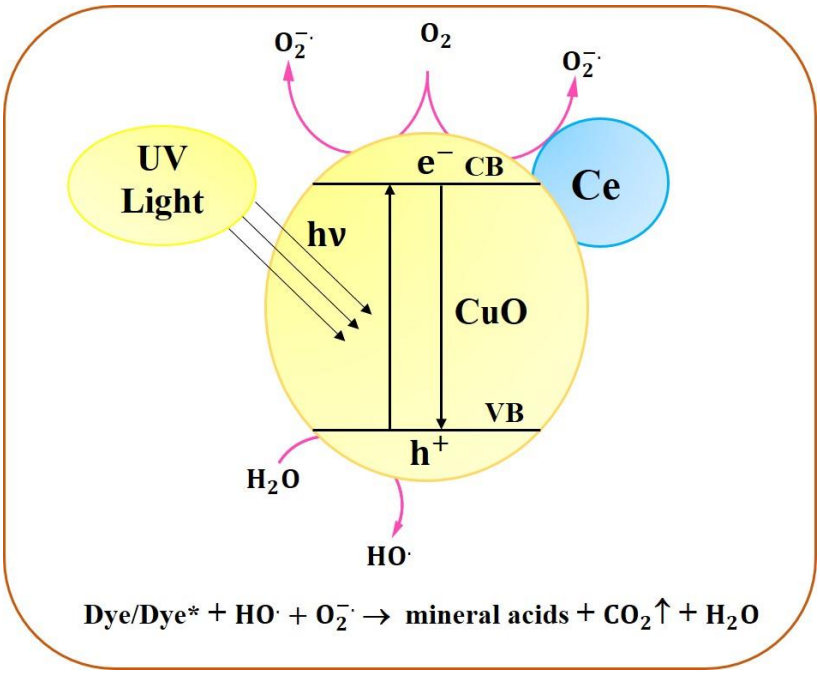

Figure 5. Photocatalytic degradation mechanism of trypan blue dye using Ce/CuO NPs [52].

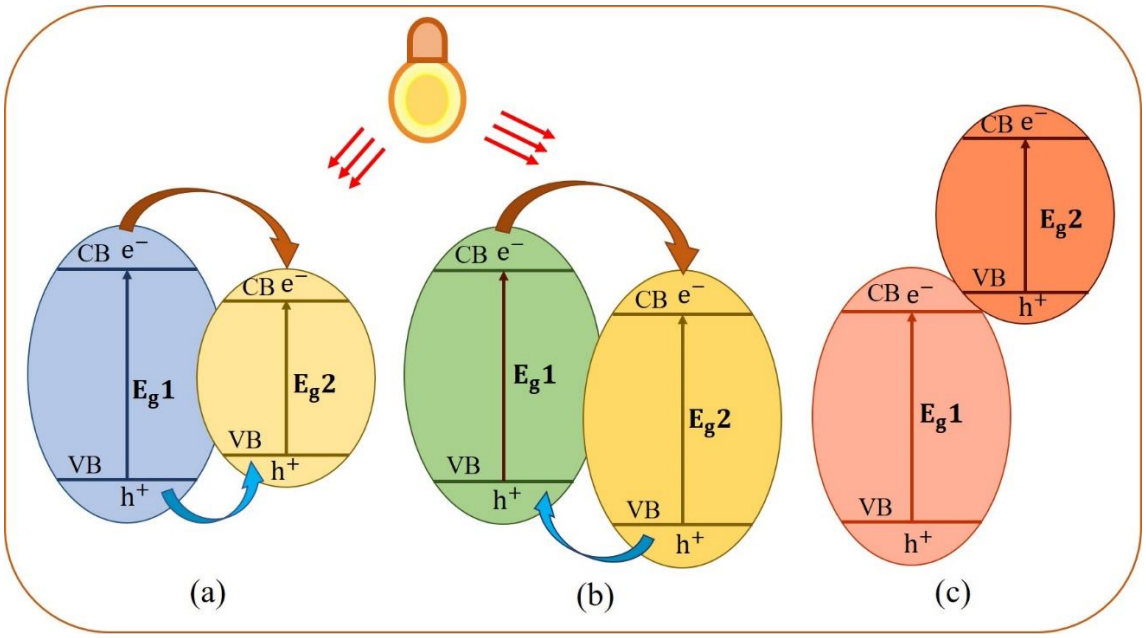

Figure 6. Possible bandgap alignment, (a) straddling band gap, (b) staggered gap, and (c) broken gap of semiconductors 1 and 2 with their respective energies, E_g1 and E_g2.

Another method of inhibiting the recombination rate of e^-/h^+ pairs in CuO are to couple it with other semiconductors with proper band gap alignment to form heterojunctions. Depending on the CB and VB potential alignments with other semiconductors, there can be three possible types of band gap intercalations. These include staggering gaps, straddling gaps, and broken gaps as illustrated in Figure 9. While in straddling bandgap alignment both CB electrons and VB holes are transferred from the wider semiconductor 1 to the narrower bandgap semiconductor 2, Figure 6 (a), in staggered gap CB electrons from semiconductor 1 with more negative potential are transferred to CB of semiconductor 2 and VB holes move in the opposite direction, Figure 6 (b). On the other hand, in broken gap configuration, Figure 9 (c), both CB electrons and VB holes of semiconductor 2 are more negative than semiconductor 1 and no charge charrier transfer from one semiconductor to the other can occur across the interface between them because of energy barrier and of the three possible bandgap alignments mentioned, type II (staggered bandgap alignment) results in better separation of charge carriers and higher degradation percentage [55].

Several studies reported on the photocatalytic proficiency of CuO-based type II heterojunctions for organic contaminants. For example, Mageshwari *et al.* [56] reported enhanced photocatalytic performance of CuO/ZnO composite for methyl orange and methylene blue dyes as compared to pure CuO and ascribed this improved performance of the composite to the enhanced charge transport and efficiency of charge carriers separation owing to intercalated band gap positions by the n-type ZnO and p-type CuO (n-p) heterojunction formation between the two oxides, Figure 7 (a), which prolongs the lifetime of photogenerated e^-/h^+ pairs and the formation of more reactive radicals and higher removal efficiency. In another study reported by Hossain *et al.* [57] it was observed that the catalytic activity of CuO/CdS nanocomposite for the photocatalytic degradation

of rhodamine B was superior (93%) as compared to the performance achieved by the individual phases of CuO and CdS which degraded the dye by 41 and 60%, respectively under the same experimental condition of initial dye concentration 30 ppm and catalyst dose of 0.25 g/L for 1 h of irradiation under visible light. The authors have reasoned the greater performance of CuO/CdS heterostructure photocatalyst than the individual phases to be owing to efficient photogenerated charge carrier separation, accelerated charge carrier transfer across the surface/solution interface, and its higher BET specific surface area. The photocatalytic degradation mechanism is shown in Figure 7 (b).

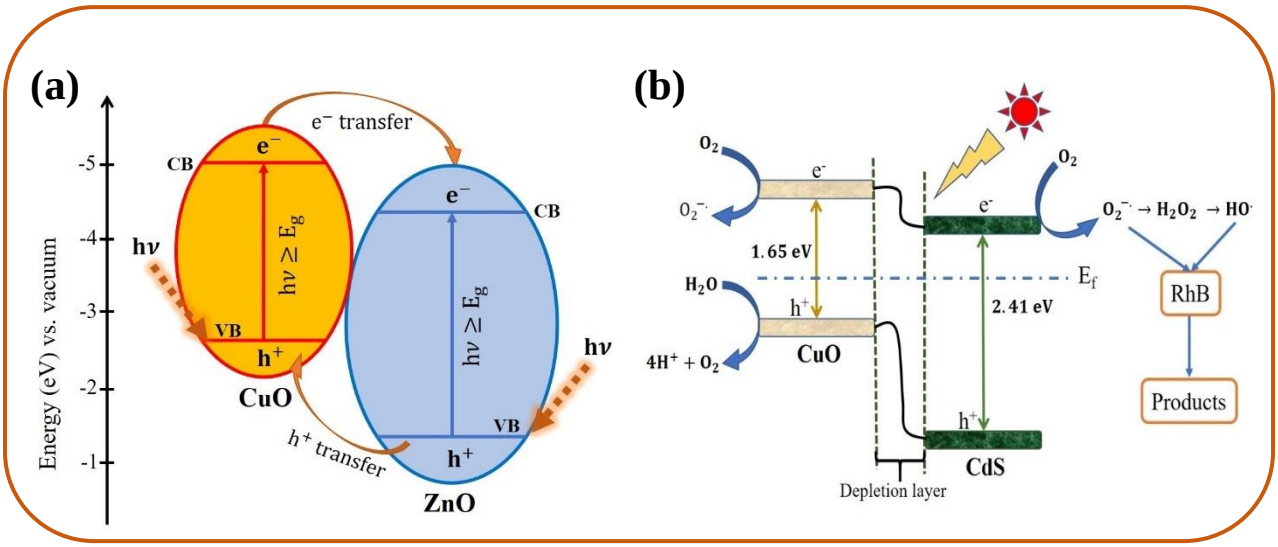

Figure 7. Illustration of e^-/h^+ formation and separation in CuO/ZnO composite (a), reprinted with permission from reference [56]. Copyright 2014. Elsevier, (b) RhB using CuO/CdS p-n heterojunction catalyst. Reprinted with permission from reference [57]. Copyright 2020. Elsevier.

However, a Z-scheme charge transfer mechanism was proposed for the observed enhanced photocatalytic activity of CuO-WO_3 heterojunction catalyst for the degradation of methylene blue dye as compared to the degradation efficiency achieved by bare WO_3 NPs [58]. Here, the type II heterojunction mechanism is not able to explain the phenomena because CB electrons in WO_3 cannot reduce O_2 to $O_2^{-\cdot}$ as the reduction potential for $O_2/O_2^{-\cdot}$ is more negative than the CB edge potential of WO_3 and VB holes in CuO cannot oxidize H_2O to $HO^{\cdot}$ because VB edge potential is more negative than the oxidation potential of $HO^{\cdot}/H_2O$, as clearly indicated by the red crossed "X" symbol in Figure 8. One advantage of the Z-scheme heterojunction over type II heterojunctions is that unlike in type II, it results in effective charge carriers separation while maintaining the redox ability of the composite because, during the transfer process, the reducing ability of CB electrons in the semiconductor with more negative potential and the oxidizing ability of the VB holes in the semiconductor with the more positive potential is not affected [59]. Therefore, Z-scheme heterojunctions avoid the drawback of reducing the redox potential during the charge transfer process observed in type II heterojunctions while maintaining the charge carrier separation efficiency. Similarly, a Z-scheme charge transfer mechanism was proposed for the enhanced visible-light-driven photocatalytic degradation of malachite green (MG) using CuO/g-C_3N_4 catalyst as compared to the pure semiconductors [60], Figure 12 (a).

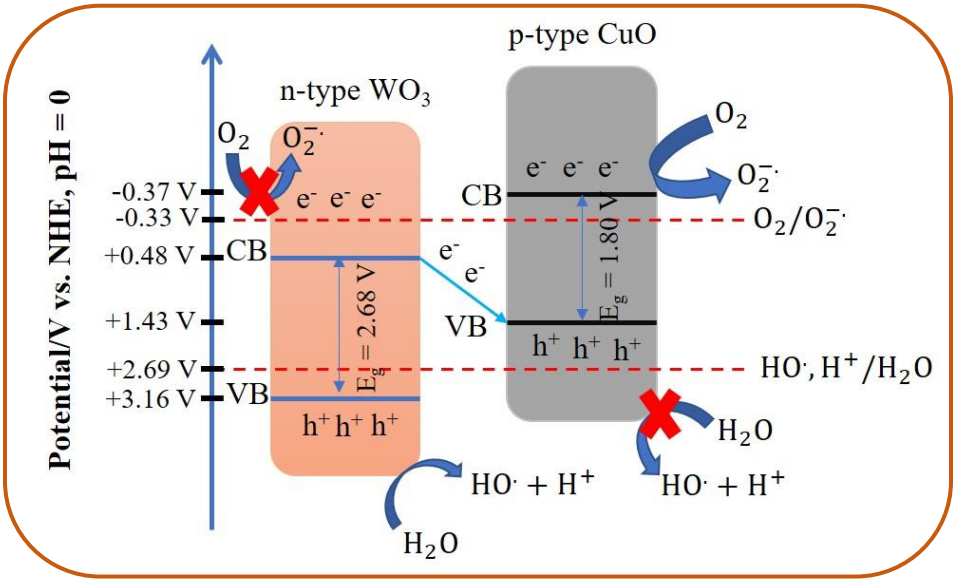

Figure 8. Electron transfer mechanism during the degradation of methylene blue using WO_3-CuO n-p heterojunction catalyst. Adapted from reference [58].

In this mechanism, VB electrons from semiconductors g-C_3N_4 and CuO are excited to their respective CB and the CB electrons in CuO move to the VB of g-C_3N_4 at the interface and CB electrons in g-C_3N_4 reduce dissolved oxygen to $O_2^{-\cdot}$ radical meanwhile VB holes in CuO oxidize H_2O or HO^- to $HO^{\cdot}$ radical, resulting in effective separation of e^-/h^+ pairs and generation of numerous reactive radicals and a higher destruction rate of the MG molecules, Figure 9 (a).

In addition to binary composites, researchers have also synthesized ternary composites to boost the photocatalytic degradation of different organic contaminants. For instance, Kumaresan *et al* [61] noticed that the photocatalytic activity of reduced graphene oxide (rGO)-based CuO/ZnO that is CuO/ZnO/rGO ternary composite exhibited catalytic activity 12 times more than that achieved by CuO/ZnO binary composite towards Rhodamine B (RhB) dye under visible light irradiation and explained that the pronounced degradation of the ternary composite compared to the binary composite is due to the excellent adsorption and charge carriers conducting properties of the rGO

in the composite. It has also been reported that the greater decomposition rate of the antibiotic tetracycline hydrochloride using rGO/CuO/Cu_2O catalyst compared to the pure phases was due to the presence of rGO which boosts the stability of CuO/Cu_2O catalyst and also acts as CB electron acceptor thereby facilitating the separation of e^-/h^+ pairs and production of more reactive radicals and higher degradation rate [62], Figure 9(b).

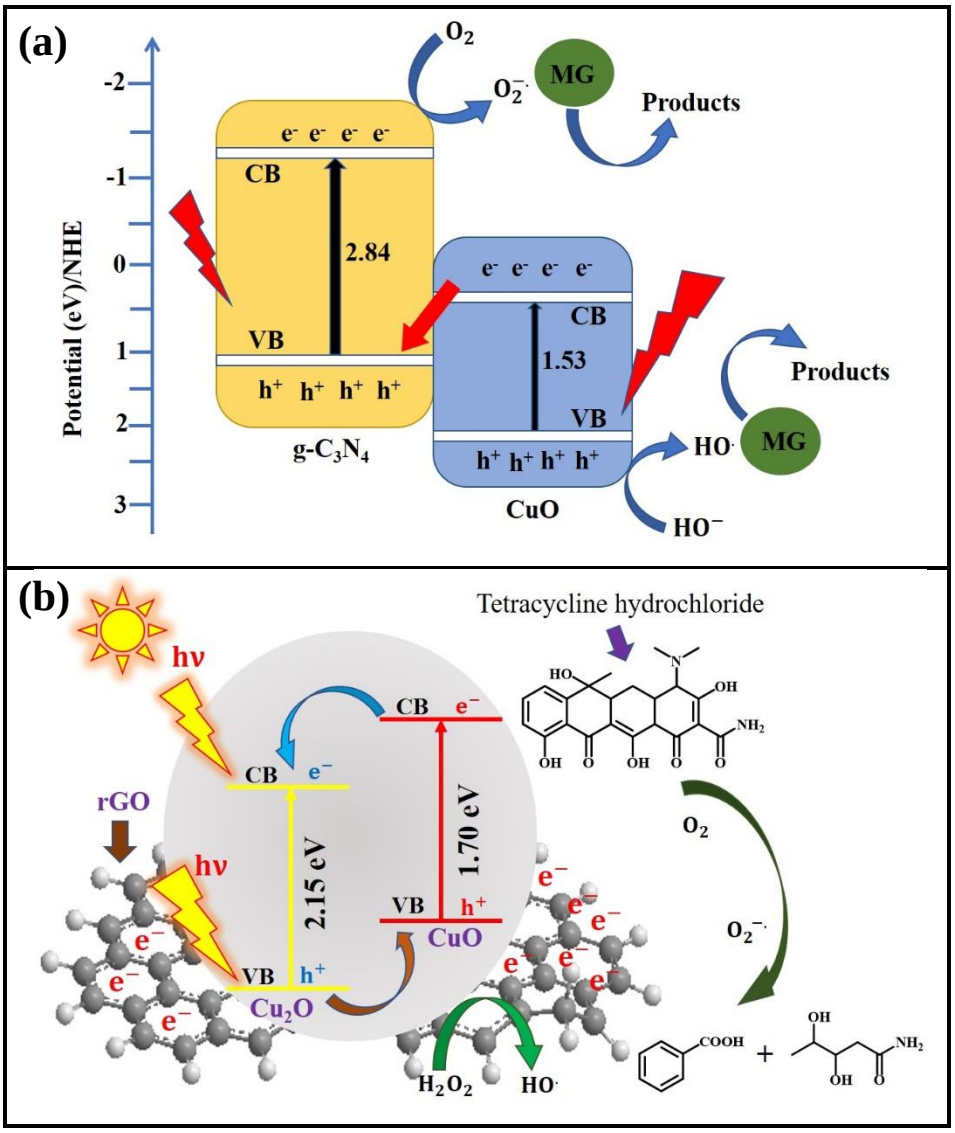

Figure 9. Band gap position and electron transfer mechanism in the degradation of (a) CuO/g-C_3N_4 composite [60] (b) Tetracycline hydrochloride using rGO/CuO/Cu_2O catalyst. Reprinted with permission from reference [62]. Copyright 2021. Elsevier.

Bajiri *et al* [63] studied the photocatalytic performance of CuO/ZnO/g-C_3N_4 ternary composite for the photocatalytic degradation of methylene blue under visible light illumination. They found about 98% removal efficiency at 45 minutes of degradation time using 100 mL of 10 ppm methylene blue and 0.04 g of catalyst and 400W hollow lamp as a light source. The authors proposed that the observed pronounced activity of the ternary composite as compared to CuO/ZnO

binary composite was due to efficient separation of photogenerated e^-/h^+ pairs by the Z-scheme charge carrier transfer mechanism.

In this Z-scheme mechanism, the photogenerated CB electrons in ZnO transfer and combine with holes in g-C_3N_4 and CuO, leaving holes in the VB. Then, the VB holes can oxidize HO^- to $HO^{\cdot}$ because they have enough potential (3.0 V) compared to the potential needed to produced $HO^{\cdot}$ (1.99 V vs. NHE at neutral pH). Moreover, the CB electrons of CuO and g-C_3N_4 are also capable of reducing O_2 to $O_2^{-\cdot}$ Because their respective redox potential -0.77 V and -1.12 V are enough to produce $O_2^{-\cdot}$ radicals (-0.046 V). Thus, they reasoned that the enhanced photocatalytic activity of the ternary composite for the organic pollutant is best explained by the Z-scheme mechanism.

In another study by Liu *et al* [64], the higher degradation of RhB using CuO nanoflower (NF)/-decorated rGO than pure CuO under UV irradiation in the presence of H_2O_2 oxidant was because of the facilitated adsorption of RhB by π-π stacking interactions between RhB and the π-conjugation system of CuONF/rGO, leading to the fast degradation of the dye. Similar higher catalytic activity for 4-nitrophenol and 2-nitrophenol pollutants using CuO/rGO catalyst than pure CuO NPs was also reported and the reason has been attributed to the good photoexcited electron

capturing ability of the graphitic backbone and also the good transfer of charge carriers, resulting in efficient separation of charge carriers and higher reactive radicals and rate of reaction [65], Figure 10. Additionally, Dutta *et al.* [66] found 99% degradation of methylene blue using CuO quantum dots decorated rGO in the presence of H_2O_2 in 50 minutes of irradiation under visible light. According to the authors, the enhanced degradation of the dye is due to excess formation of $HO^{\cdot}$ and $O_2^{-\cdot}$ reactive radicals' production by the visible-light-induced excitation of elections from rGO and transferring to the CB of CuO, resulting in more radicals' production and improved

degradation reaction rate. Similar enhanced removal of methylene blue and Congo red dyes using rGO-CuO catalyst under visible light illumination was also recently reported by our group [67].

Similar to elemental doping, coupling CuO with other semiconductors may not necessarily result in enhanced photodegradation rather consideration of other factors such as resulting bandgap and surface area of catalyst need to be taken into consideration to explain the experimentally observed degradation efficiency. For example, in a study reported by Koohestani [68], the degree of elimination of methyl orange using pure CuO NPs was found to be higher than Cu_2O/CuO mixture. According to the author, this could be due to the smaller bandgap and larger specific surface area of CuO NPs than the Cu_2O/CuO photocatalyst.

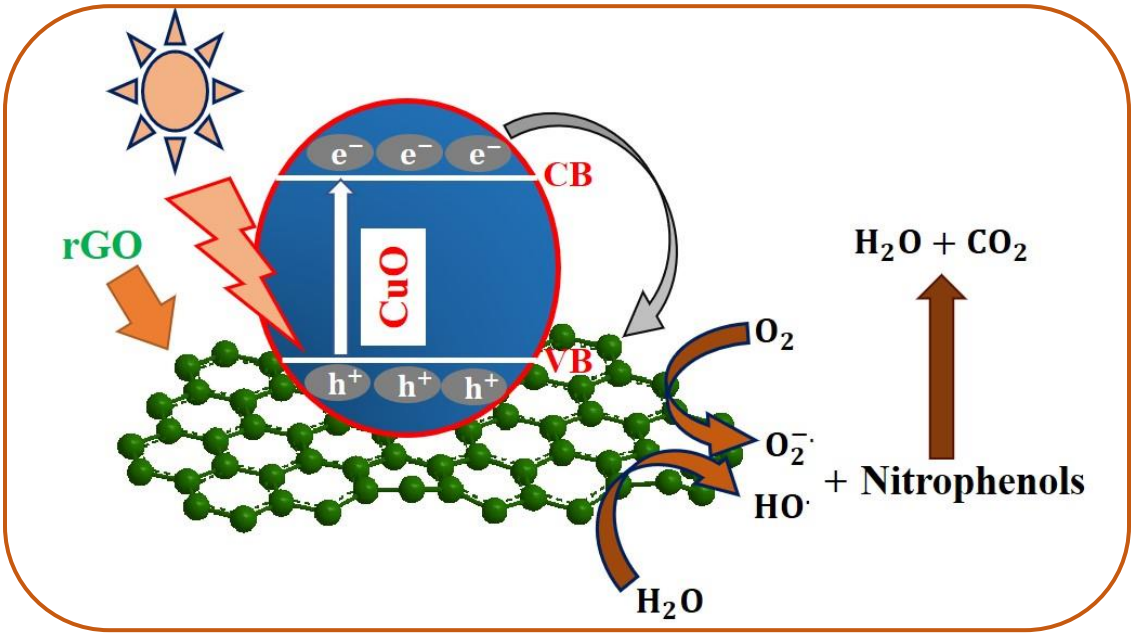

Figure 10. Illustration of electron transfer mechanism in CuO/rGO composite during the degradation of RhB dye. Adapted from reference [65].

2.3.2 Effect of type of catalyst and organic pollutant

The photocatalytic degradation percentage of organic contaminants in aqueous media is potentially influenced by the nature of catalyst as well as the organic contaminants keeping other variables unchanged. The photocatalytic activity response of a given catalyst to different pollutants can vary depending on the nature of the pollutants. This variation may generally be attributed to disparity in molecular mass, molecular structure and stability, and molecular charges at the pH of the reaction suspension. Several researchers have reported the performance of CuO and CuO-based catalysts for the photocatalytic destruction of various organic contaminants. For example, Singh *et al* [69] studied the catalytic activity of CuO nanorods synthesized by sol-gel method to the degradation of methyl orange, methylene blue, Eriochrome Black T, and Congo red dyes individually and under similar experimental conditions and they found removal percentages in increasing order: Congo red < methylene blue < Eriochrome Black T < methyl orange. This observed discrepancy of degradation performance of the same catalyst to Congo red (M_w = 696.7 g/mol) with the slowest rate of degradation as opposed to methyl orange (M_w = 327 g/mol) with the highest rate was attributed to their variation in molecular mass of the dyes (indicated in Figure 14) which results in different diffusion rate to catalyst surface active sites and hence the rate of decomposition reaction. In another study, the extent of degradation of Nile blue was found to be 97% while that of reactive yellow 160 was 80% under sunlight irradiation for 2 h utilizing the same biosynthesized CuO NPs catalyst [70]. A similar explanation that is based on the variation in the diffusion rate to catalyst surface active sites owing to the difference in molecular mass and structure of the dye molecules, Figure 15, was offered to the observed disparity in catalytic performance. Moreover, methylene blue was degraded by 39% as compared to 28% of methyl orange under visible light irradiation for a period of 2h using the same ZnO/CuO (50:50) photocatalyst [71]. In a study conducted by using the same 10 ppm pollutant concentration for 320

minutes of irradiation under sunlight at their respective natural pH and catalyst dose of 10 mg/L of biosynthesized CuO NPs for six different pollutants of methyl red, Congo red, methylene blue, trypan blue, methyl orange, and Coomassie brilliant blue, the respective degradation percentages obtained were 77.4, 77.7, 79.6, 72.04, 59.9, and 43.6 % [72]. In a different investigation, a comparison of the degradation of methylene blue, methyl red and Congo red dyes taken individually using electrochemically synthesized CuO NPs and a similar amount of catalyst and dye concentration under sunlight illumination for a period of 2 h resulted in degradation of 93, 90, and 85%, respectively [73]. The rate constant of the reactions was different with the highest value of 0.02059 min^{-1} belonging to the degradation of methylene blue and the lowest 0.01749 min^{-1} for Congo red and the authors have explained the observed lowered rate of degradation of Congo red to be due to its less susceptible chemical structure to oxidation and also steric hindrance originating from the biphenyl group and naphthenic groups in its structure.

Nevertheless, the explanation by molecular mass difference alone may not necessarily account for the experimentally observed difference in the removal efficiency of dyes employing the same catalyst. For example, it has been reported by Hossain *et al.* [57] that the removal percentages of rhodamine B, methylene blue, methyl blue, and methyl orange dyes utilizing CuO/CdS composite catalyst were 93%, 75%, 83%, and 80%, respectively which is unlike to their order in molecular masses which is 479, 319.85, 800, and 327 g/mol, respectively. Thus, other factors such as molecular structural complexity and stability including the ionicity of the molecules at the experimental pH should also be taken into consideration to account for the observed variation in degradation competence.

The elimination rate of a given organic pollutant using CuO and CuO-based catalysts also depends on the type of catalyst. This could be primarily a result of the associated variation in band gap energy and morphology of the particles as discussed previously. A case in point is the degradation of phenanthrene using $Gd_2O_2CO_3$/CuO/ZnO nanocomposite exhibited a higher removal rate of 99.6 % during 2 h of illumination time under visible light as compared to 50.4% when pure CuO was used for the same time duration [74]. This enhanced performance of the ternary nanocomposite was attributed to its high light absorption, high surface area, and reduced recombination rate of charge carriers. Additionally, the degradation rate of methylene blue and methylene violet dyes taken separately using Zn-doped CuO nanoflowers was higher than utilizing pure CuO at comparable other experimental parameters [75]. It has been suggested that the enhanced activity of the Zn-doped CuO relative to CuO was because of the efficient photogenerated e^-/h^+ pairs separation as a result of the Zn atoms acting as CB electron traps and a hence larger number of reactive radicals' production and degree of removal of the dyes.

2.3.3 Effect of catalyst dose and pollutant initial concentration

The initial catalyst dose and pollutant concentration employed are among the operational parameters that affect the removal efficiency of organic pollutants. Generally, heterogeneous photocatalytic reactions are effective at the optimal amount of catalyst dose and dye concentration. Regarding pollutant concentration, photocatalytic reactions are efficient at lower concentrations because higher concentrations prevent radiation penetration and obscure catalyst active sites thereby minimizing the number of reactive radical species that would have been produced and hence suppress the rate of the degradation process. Similarly, using a catalyst amount above optimal could form a suspension that occludes radiation from passing through and fosters particle

agglomeration which in turn tends to reduce the number of active surface sites and the rate of the decomposition process. Utilizing the below optimal amount of catalyst will also decrease the extent of degradation for a lower number of surface-active sites for the formation of reactive species will be produced. Thus, the influence of dye initial concentration and catalyst dose on the removal efficiency of pollutant compounds are among the important operational parameters that are studied and optimized in many photocatalytic degradation reactions. To mention some, Venkata *et al.* [76] studied the impact of varying the initial concentrations of Coomassie Brilliant Blue R-250 and methylene blue dyes separately from 5 to 25 ppm in intervals of 5 ppm employing a fixed catalyst loading of 10 mg and pH of 7 under sunlight irradiation. They observed that the degradation decreased with a rise in dye concentration in both dyes and attributed this phenomenon to increased coverage of surface-active sites with dye molecules, resulting in a reduced rate of reactive species production and hence decomposition. Moreover, the authors also observed that increasing catalyst dose from 5 – 25 mg keeping other variables fixed resulted in respective maximum degradation percentages of 74 and 86% but any further addition of the catalyst above 25 mg lowered the degradation. This has been ascribed to particle aggregation and solution turbidity which result in a reduction in surface active sites and blockage of radiation, respectively and hence lower destruction of the dyes. Akram *et al.* [77] studied the effect of $Co(OH)_2$/CuO catalyst dose by varying from 5 – 20 mg in intervals of 5 mg and rhodamine B dye initial concentration from 25 – 100 mg/L in intervals of 25 mg/L on the percentage of degradation and found maximum value of 99.9% at 10 mg catalyst dose and 25 mg/L dye initial concentration. Keeping other experimental parameters unchanged, increasing catalyst loading above 10 mg or dye initial concentration above 25 mg/L hindered degradation probably because both cases result in scattering or obstruction of radiation which in turn results in ineffective production of reactive

radicals and lowered rate of degradation. In another study reported by Date *et al* [78], The photocatalytic performance of CuO/TiO_2 hybrid nanorod arrays was consistently decreased with an increase in rhodamine B initial concentration from 50 to 250 and then to 750 ppm in the presence of H_2O_2 oxidant and without varying other experimental parameters. According to the authors, the enhanced activity of the hybrid photocatalyst relative to bare CuO was due to the formation of type II heterostructure between CuO and TiO_2, which results in more efficient separation of charge carriers and the formation of more $HO^{\cdot}$ and $HOO^{\cdot}$ radicals generated from H_2O_2 via its reaction with photogenerated e^-/h^+ pairs in a process called photo-Fenton-catalysis and therefore a greater degradation rate. Similarly, the influence of Direct red 89 initial concentration on the photocatalytic activity of Fe_3O_4/CuO core-shell heterostructure under visible light irradiation was studied by Benabbas *et al.* [79]. They found that nearly complete removal of the dye was achieved utilizing its initial concentration in the range from 20 – 60 ppm and catalyst dose of 0.75 g and 100W visible light irradiation at the experimental pH of 6 for 240 min. However, degradation decreased upon increasing the initial concentration from 40 – 60 ppm while other parameters are kept fixed. As mentioned previously, the authors have reasoned this to be due to suppressed rate of radical formation as a result of coverage of catalyst surface active sites by dye molecules at higher concentration as well as radiation screening effect of dye molecules, both of which result in reduced generation rate of radicals and rate of degradation reaction. A consistent reduction in the rate of destruction of methylene blue up on increasing its initial concentration from 5 to 20 ppm using CuO/ZnO nanocomposite catalyst was also reported by Sakib *et al.* [80]. In a study reported by Abdullah *et al.* [81] for the photocatalytic degradation of methylene blue using CuO-$BiVO_4$ catalyst, while the percent of decomposition of the dye monotonically lowered with the rise in its concentration from 10 to 30 ppm in intervals of 5 ppm without changing other

experimental variables, the degradation increased and reached maximum value upon increasing catalyst dose from 0.2 to 0.8g in intervals of 0.2 g but further increment above 0.8 to 1 g did not change significantly. Table 1 provides additional examples of degradation efficiency achieved by CuO and CuO-based photocatalysts for the degradation of different organic pollutants at the indicated experimental parameters as reported from various references.

Table 1. Effect of catalyst dose and pollutant concentration on the removal efficiency of various organic pollutants in an aqueous solution.

Pollutant	[Pollutant] (ppm)	Catalyst	Catalyst dose (g)	Conditions	D (%)	Ref.
4-Nitrophenol	10	CuO/rGO	0.03	pH = 8.1, t = 2 h, under visible light	100	[65]
4-Nitrophenol	10	CuO	0.03	pH = 8.1, t = 2 h, under visible light	72	[65]
Acid Fuchsin	20	CuO/MnO_2	Single film	V = 3 mL, 0.05 mL H_2O_2, 0.45 mL H_2O, t = 8h,	94.1	[82]
Acid Fuchsin	20	CuO/MnO_2	Single film	V = 3 mL, 0.05 mL H_2O_2, 0.45 mL H_2O, t = 8h,	72.5	[82]
Methylene blue	10	1wt% $CuO-BiVO_4$	0.8	V = 1L, pH = 10, t = 4h, under 18W visible light	100	[81]
Rhodamine B	0.0105	$Co(OH)_2/CuO$	0.02	V = 50 mL, pH = 7, t = 8 min., using UV light	99.9	[77]
Methylene blue	10	CuO/Co_3O_4	---	V = 50 mL, t = 3h, using 500 W Xe lamp	56	[83]
Methylene blue	10	CuO	---	V = 50 mL, t = 3h, using 500 W Xe lamp	40	[83]

Methylene blue	40	CuO/MgO	1.0	V = 100 mL, pH = 2.2, t = 80 min., using UV light	96	[84]
Phenanthrene	20	$Gd_2O_2CO_3$/ZnO/CuO	0.4 g/L	V = 100 mL, pH = 4, t = 2 h, using visible light	99.6	[74]
Methylene blue	15	0.07M Zn-CuO	0.005	t = 3 h, using visible light	~ 100	[85]
Methylene violet	15	0.07M Zn-CuO	0.005	t = 3 h, using visible light	~ 100	[85]
Methylene blue	100	Ag@CuO/PAA	0.1	V = 100 mL, t = 30 min, under sunlight	99.0	[86]
Rhodamine B	10	CuO/Fe_2O_3	0.04	V = 80 mL, t = 1hr,	100	[87]
Direct red 89	20	Fe_3O_4/CuO	0.75	V = 250 mL, 7 mL H_2O_2 added, t = 240 min., using 100W visible lamp	~ 100	[79]
Aniline	100	CuO	0.05 g/L	t = 1 h, pH = 7, using 30W UV-C lamp	78	[88]

2.4 Photocatalytic activity of CuO NPs for removal of toxic metal ions

In addition to organic pollutants, inorganic pollutants are also common in discharged effluents from various industries. These include heavy metals, sulfates, cyanides, mineral acids, etc and can pollute water if available in higher than permissible limits [89]. Removal of toxic heavy metal ions is crucial to ensure their safety to humans and the environment. Heavy metal ions such as Ni^{2+}, Hg^{2+}, Pb^{2+}, As^{3+}, Cd^{2+}, Cr^{6+} are among the contaminants listed under priority pollutants by the United States Environmental Protection Agency (USEPA), and as such a maximum allowable limit of these ions in wastewater, soil for agriculture, and drinking water has been stipulated by different

organizations. For instance, the World Health Organization (WHO) has set recommended safe concentration limit of some heavy metals such as Hg^{2+}, Cd^{2+}, Pb^{2+}, Cr^{6+}, and Ni^{2+} in wastewater equal to 0.001, 0.003, 0.01, 0.05, and 0.02 ppm, respectively [90]. Since consumption of these metal ions from different sources in humans can induce multifarious health problems principally by replacing the nutritional metals of organic cells in our body and inhibiting their function and also dysfunction our vital organs such as kidney, liver, nervous system, the brain function and could even cause death they should be controlled and managed and removed from their sources mainly those effluents from industrial wastewater to meet stringent discharge standards [91]. Moreover, metal ions are not biodegradable and discharges of low concentration of these ions can lead to their enrichment over long-term accumulation via the food chain and drinking water and therefore heavy metal ion recovery via photocatalytic reduction may be the best option to address the specified problems [92, 93]. Photocatalytic reduction is also one alternative approach to recovering precious metals such as platinum, silver, and gold from wastewater effluents. Table 2 gives the most common toxic heavy metal ions with the toxicity they induce to humans and the environment as well as the toxicity limit set by different organizations in agricultural soils, drinking water, and industrial effluents.

For these metal ions to be reduced to an elemental or lower valency state by the CB electrons of the semiconductor, the reduction potential of the metal should be more positive than the CB edge potential of the semiconductor being used. The standard reduction potential of the most toxic metal ions and metalloid arsenic ion in water at 25 ^{o}C vs NHE is given in Eq. (20-25).

$$Pb^{2+}(aq) + 2e^{-} \rightarrow Pb(s) \qquad E^{0} = -0.13\ V \qquad (20)$$

$$Hg^{2+}(aq) + 2e^{-} \rightarrow Hg(l) \qquad E^{0} = +0.85V \qquad (21)$$

$$Cd^{2+}(aq) + 2e^- \rightarrow Cd(s) \qquad E^0 = -0.40\ V \qquad (22)$$

$$Ni^{2+}(aq) + 2e^- \rightarrow Ni(s) \qquad E^0 = -0.26\ V \qquad (23)$$

$$H_3AsO_4(aq) + 2e^- \rightarrow H_3AsO_3(aq) \qquad E^0 = +0.56\ V \qquad (24)$$

$$Cr_2O_7^{2-}(aq) + 14H^+(aq) + 6e^- \rightarrow 2Cr^{3+}(aq) + 7H_2O; \quad E^0 = +1.33\ V \qquad (25)$$

Similarly, for the metal ions to be oxidized to a higher valence state, the oxidation potential of photogenerated holes should be more positive than the oxidation potential of the metal ions. For example, Pb^{2+} has been removed by reacting with available HO^- forming $Pb(OH)_2$ precipitates or getting oxidized to PbO_2 via reaction with h^+ or $HO^{\cdot}$ and reacting with dissolved O^{2-} thereby changing its oxidation state to Pb(IV), Eq. (26) [94].

$$Pb^{2+} \rightarrow Pb^{4+} + 2e^- \qquad E^0 = -0.67\ V \qquad (26)$$

Chromium (Cr) can exist principally in hexavalent Cr(VI) or trivalent Cr(III) oxidation states in soils and aqueous environment and while Cr(VI) is toxic, cancerogenic and mutagenic contaminant, Cr(III) is vital micronutrient for the human body [95]. Therefore, reducing the oxidation state from VI to III is a safe method used to avoid the toxicity associated with chromium compounds in aqueous media. Similar to chromium, arsenic primarily occurs in arsenite (As (III)) and arsenate (As(V)) oxidation states of which As (III) is the prevalent form it exists in groundwater and is much more toxic than As (V) and as such one viable option to avoid its toxicity will be to oxidize it to its less toxic oxidation state [96].

Several reports in the literature emphasized the photocatalytic reduction of toxic heavy metal ions using CuO and CuO-based photocatalysts. For example, almost complete reduction of chromium from Cr(VI) to Cr(III) valence state has been achieved via photoreduction using the mesoporous

CuO/ZrO_2-MCM-41 nanocomposite catalyst in 30 minutes [97]. In another study, 100% photoreduction of 100 ppm of Cr(VI) to Cr(III) was achieved using TiO_2/rGO/CuO ternary composite as photocatalyst in 80 minutes under visible light irradiation [95]. The photocatalytic reduction of Cr(VI) using CuO nanoparticles together with different organic acids under simulated solar illumination was also reported [98].

Table 2. List of toxic heavy metal ions, their maximum contaminant level as set by different organizations and their toxicity. [a] = USEPA; [b] = WHO; [c] = European Union (EU).

S/N	Heavy metal ion	Maximum concentration limit (mg/L)			Toxicity	Ref.
		Drinking water	Agriculture soils	Wastewater		
1	Hg^{2+}	0.002[a], 0.001[c]	0.050[b]	0.00003[a], 0.001[b], 0.005[c]	Kidney disease, disease of circulatory and nervous system	[99,100]
2	Pb^{2+}	0.015[a], 0.010 [b, c]	0.100[b]	0.006[a], 0.010[b]	Digestive problems, high blood pressure, kidney, circulatory, and nervous system diseases, memory problem in adults	[100, 101]
3	Cd^{2+}	0.005[a, c], 0.003[b]	0.003[b]	0.010[a], 0.003[b]	Human carcinogen, kidney, renal, cardiovascular, central and peripheral system, reproductive and respiratory system damage	[99,100]
4	As^{3+}	0.010[b],	---	0.050[a]	Causes cancer in skin, lung, and bladder	[102]

5	Cr^{6+}	0.050[a]	0.100[b]	0.050[a], 0.050[b]	Kidney, liver, nervous system damage, lung cancer, bone cancer, diarrhea, and dermatitis	[103]
6	Ni^{2+}	---	0.05b	0.20[a], 0.02[b]	Dermatitis, allergy, respiratory system cancer	[104]

Sun *et al.* [105] has reported the photocatalytic oxidation of arsenite (AsO_3^{3-}) to arsenate (AsO_4^{4-}) using CuO-Fe_3O_4 nanoparticles under visible light illumination. Ahamed *et al.* [106] observed about 95% removal of Ni^{2+} ions from aqueous solution using TiO_2/CuO thin film under visible light irradiation for 45 minutes. This removal performance, which was higher by 17% compared to the achievement when CuO thin film is used in the same time duration was ascribed to the better separation efficiency of photogenerated electrons and holes in the heterojunction composite which enables photoexcited electrons to react with adsorbed Ni^{2+} and reduce it to elemental Ni.

Nogueira *et al.* [107] reported pronounced photocatalytic reduction of Cr (VI) to Cr(III) using Nb_2O_5/CuO (10wt%) heterostructure with a removal efficiency of 78% versus 23% when a mechanical mixture of the pure oxides was employed under visible light irradiation for 210 minutes. The formation of type-II heterostructure between the two oxides which results in effective charge carriers' separation due to the transfer of CB electrons from CuO to the CB of Nb_2O_5, Figure 11(a) and higher absorption in the visible region has been proposed to be the reason for the superior removal percentage observed. In another report by Yu *et al.* [108], virtually complete reduction of Cr^{6+} in aqueous solution upon irradiation under visible light for 80 minutes was found employing CuO/ZnO composite and this was higher than that achieved by the pure oxides individually under similar conditions. However, a removal efficiency of only 55% was achieved during the photocatalytic reduction of the same ion specified using Cu-TiO_2/CuO photocatalyst

under solar light irradiation for 4h [109]. While in a study conducted by Kadi *et al al.* 100% removal of Hg^{2+} via photocatalytic reduction using 1.6 g/L 2%CuO/g-C_3N_4 catalyst loading in 30 minutes under visible light irradiation was reported.

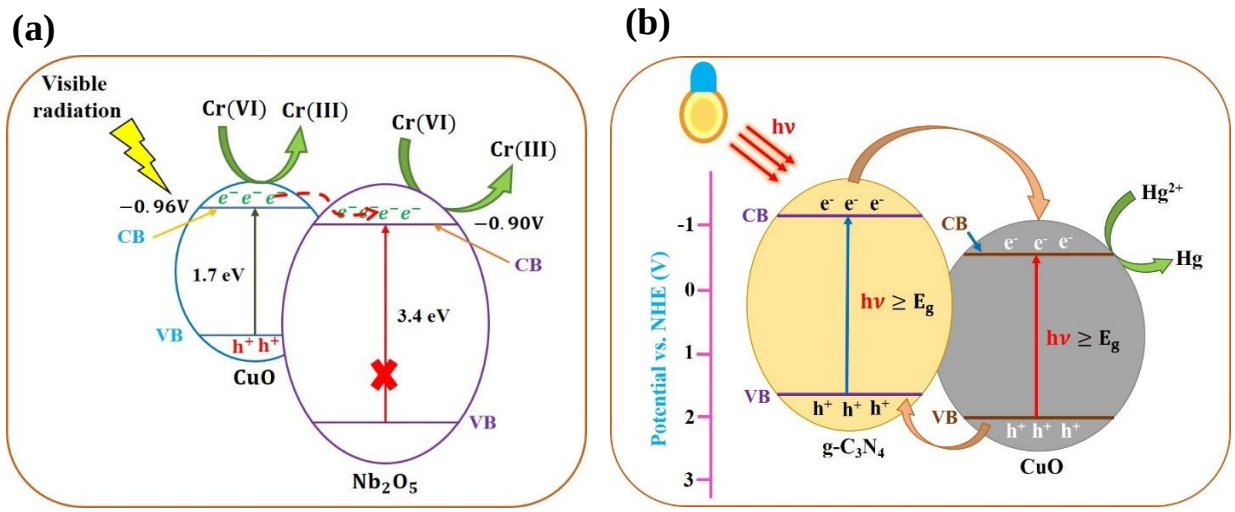

Figure 11. Removal via photocatalytic reduction of Cr^{6+} using Nb_2O_5/CuO heterostructure (a) [107] and Hg^{2+} using CuO/g-C_3N_4 mesoporous heterostructure photocatalyst (b) [110].

This performance achieved by the mesoporous composite catalyst was higher than that of the pure phases individually and attributed the observed enhanced performance to effective e^-/h^+pairs separation by the formation of heterojunction between CuO and g-C_3N_4, Figure 11(b), dispersing of small particles of CuO onto g-C_3N_4 having large surface area and small bandgap, rapid transfer of the Hg^{2+} ion to the catalyst surface and also minimized light scattering owing to the mesoporous structure of the catalyst. Similar higher performance photocatalytic removal of Pb^{2+} from aqueous solution using graphene–CuO nanocomposites as compared to pure CuO or mechanically mixed graphene and CuO nanoparticles were observed by Prashanti *et al.* [111].

In addition, 100% removal of Hg^{2+} was achieved using 3% mesoporous CuO/ZnO nanocomposite in 60 minutes under visible light irradiation which was much higher than that

achieved by commercial P-25 catalyst and pure ZnO nanoparticles, as reported by Mohamed *et al.* [112]. The reason for the enhanced photocatalytic reduction of Hg^{2+} was attributed by the researchers to be due to increased surface area and pore volume which promotes mass diffusion and provides more active sites, and enhanced transfer of photogenerated charge carriers as a result of the p-n heterojunction formation between p-type CuO and n-type ZnO NPs. The charge transfer mechanism as illustrated in Fig.12 was proposed to be S-type. In this mechanism, reduction reaction, in this case reduction of Hg^{2+} to elemental Hg occurs on the CB of the semiconductor with more negative CB edge meanwhile oxidation reaction occurs on the VB of the semiconductor with the more positive CB potential, in contrast to type-II heterojunction, and that the advantage of S-type mechanism over type II mechanism is that unlike the latter, in the former case the redox potential of the semiconductors is not affected when the charge carrier transfer occurs [113].

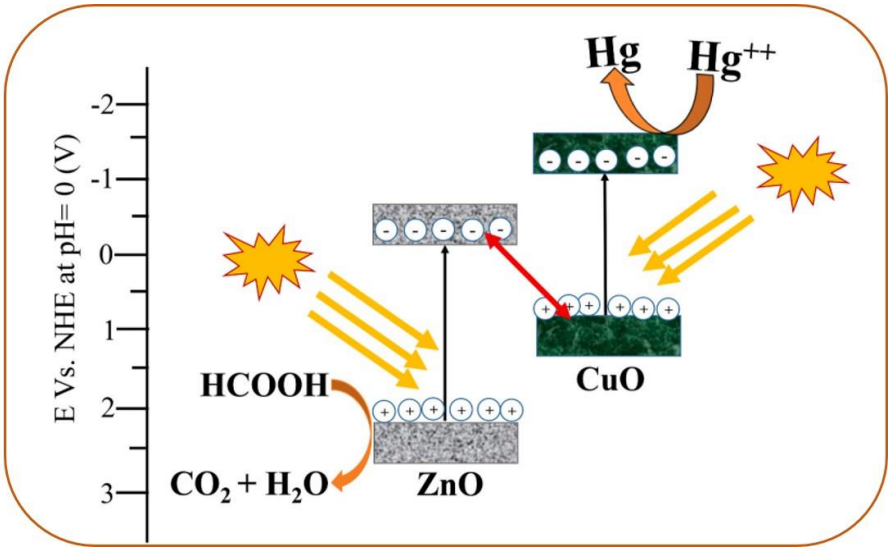

Figure 12. S-scheme heterojunction composite for the removal of Hg^{2+}using p-CuO/n-ZnO heterojunction [113].

3 Conclusions

CuO is p-type I-VI transition metal semiconductor oxide with multiple optical and electrical properties. It has a narrow bulk indirect bandgap of 1.20 eV which absorbs a visible wavelength of 1034 nm. It is used in multifarious applications including in magnetic storage media, in high-temperature superconductors, in electrodes in dye-sensitized solar cells, fuel cells, chemical and gas sensors, as an antimicrobial agent, and in the heterogeneous photocatalytic decomposition of organic pollutants as well as reduction of toxic metal ions in water and wastewater treatment. However, the photocatalytic activity response of CuO NPs is limited by its narrow bandgap which results in a greater recombination rate of charge carriers and suppressed degradation proficiency. Primarily, these limitations are overcome by means of elemental doping or coupling with other semiconductors or CuO decorated support substances. In this case, its degradation efficiency is enhanced as a result of improved properties such as increased stability, raised surface area, and dispersibility of the catalyst particles in aqueous media as well as effective separation of e^-/h^+ pairs followed by generation of enough reactive radicals and then enhanced degradation rate of pollutants. While doping with elements retards the recombination rate of photogenerated charge carriers by acting as traps for CB electrons, coupling with other semiconductors to form heterojunctions enhances degradation because of better charge carrier separation as a result of the heterojunction, especially type-II heterostructure, formed between the two semiconductors. However, the main shortcoming with type-II heterostructures is the reduction in the redox potential of the coupled semiconductors when conduction band electrons with higher CB edge potential diffuse into the other semiconductor with lower CB edge potential and VB holes in the reverse direction. In Z-scheme and S-scheme charge transfer mechanisms, the redox potential of the coupled semiconductors is maintained while effectively separating the charge carriers.

Further, the photocatalytic reduction mechanism of eradicating toxic metal ions is another potential application of photocatalysis. In this case, instead of degradation, the oxidation state of metal ions in aqueous media is reduced to lower valence or to elemental state and this way their toxicity is minimized. As compared to another common method of removing toxic metal ions, the photocatalytic approach is promising in that it is eco-friendly, low cost, and under appropriate conditions eliminates toxic metal ions from aqueous media. It is also one viable option for retrieving precious metals such as silver, gold, and platinum from wastewater.

Conflict of interest

The authors declare no potential conflict of interest regarding the publication of this work.

Acknowledgements:

The authors acknowledge support from the ERC Grant Surface-Confined fast modulated Plasma for process and Energy intensification (SCOPE) from the European Commission with the Grant No. 810182.

References

[1] N. Khatri, S. Tyagi, Influences of natural and anthropogenic factors on surface and groundwater quality in rural and urban areas, Frontiers in Life Science, 8 (2015) 23-39.

[2] W.H. Organization, Drinking water, in, 2019.

[3] N. Muhd Julkapli, S. Bagheri, S. Bee Abd Hamid, Recent Advances in Heterogeneous Photocatalytic Decolorization of Synthetic Dyes, The Scientific World Journal, 2014 (2014) 692307.

[4] G. Crini, E. Lichtfouse, Advantages and disadvantages of techniques used for wastewater treatment, Environmental Chemistry Letters, 17 (2019) 145-155.

[5] J.A. Garrido-Cardenas, B. Esteban-García, A. Agüera, J.A. Sánchez-Pérez, F. Manzano-Agugliaro, Wastewater Treatment by Advanced Oxidation Process and Their Worldwide Research Trends, International Journal of Environmental Research and Public Health, 17 (2020) 170.

[6] D. Rajamanickam, M. Shanthi, Photocatalytic degradation of an organic pollutant by zinc oxide–solar process, Arabian Journal of Chemistry, 9 (2016) S1858-S1868.

[7] C.G. Joseph, G. Li Puma, A. Bono, D. Krishnaiah, Sonophotocatalysis in advanced oxidation process: A short review, Ultrasonics Sonochemistry, 16 (2009) 583-589.

[8] G.K. Weldegebrieal, Synthesis method, antibacterial and photocatalytic activity of ZnO nanoparticles for azo dyes in wastewater treatment: a review, Inorg Chem Commun, 120 (2020) 108140.

[9] A. Pareek, S. Venkata Mohan, Chapter 1.4 - Graphene and Its Applications in Microbial Electrochemical Technology, in: S.V. Mohan, S. Varjani, A. Pandey (Eds.) Microbial Electrochemical Technology, Elsevier, 2019, pp. 75-97.

[10] N.R. Dhineshbabu, V. Rajendran, N. Nithyavathy, R. Vetumperumal, Study of structural and optical properties of cupric oxide nanoparticles, Applied Nanoscience, 6 (2016) 933-939.

[11] I.M. Tiginyanu, O. Lupan, V.V. Ursaki, L. Chow, M. Enachi, 3.11 - Nanostructures of Metal Oxides, in: P. Bhattacharya, R. Fornari, H. Kamimura (Eds.) Comprehensive Semiconductor Science and Technology, Elsevier, Amsterdam, 2011, pp. 396-479.

[12] Y. Wang, S. Lany, J. Ghanbaja, Y. Fagot-Revurat, Y. Chen, F. Soldera, D. Horwat, F. Mücklich, J. Pierson, Electronic structures of Cu_2O, Cu_4O_3, and CuO: A joint experimental and theoretical study, Physical Review B, 94 (2016) 245418.

[13] D.S. Murali, S. Aryasomayajula, Thermal conversion of Cu_4O_3 into CuO and Cu_2O and the electrical properties of magnetron sputtered Cu_4O_3 thin films, Applied Physics A, 124 (2018) 279.

[14] G.K. Weldegebrieal, Photocatalytic and antibacterial activityof CuO nanoparticles biosynthesized using Verbascum thapsus leaves extract, Optik, 204 (2020) 164230.

[15] M. Aminuzzaman, L.M. Kei, W.H. Liang, Green synthesis of copper oxide (CuO) nanoparticles using banana peel extract and their photocatalytic activities, AIP Conference Proceedings, 1828 (2017) 020016.

[16] N. Verma, N. Kumar, Synthesis and Biomedical Applications of Copper Oxide Nanoparticles: An Expanding Horizon, ACS Biomaterials Science & Engineering, 5 (2019) 1170-1188.

[17] S.A. Akintelu, A.S. Folorunso, F.A. Folorunso, A.K. Oyebamiji, Green synthesis of copper oxide nanoparticles for biomedical application and environmental remediation, Heliyon, 6 (2020) e04508-e04508.

[18] D. Vaidehi, V. Bhuvaneshwari, D. Bharathi, B.P. Sheetal, Antibacterial and photocatalytic activity of copper oxide nanoparticles synthesized using Solanum lycopersicum leaf extract, Materials Research Express, 5 (2018) 085403.

[19] A. Tadjarodi, O. Akhavan, K. Bijanzad, Photocatalytic activity of CuO nanoparticles incorporated in mesoporous structure prepared from bis(2-aminonicotinato) copper(II) microflakes, Transactions of Nonferrous Metals Society of China, 25 (2015) 3634-3642.

[20] Y.-K. Phang, M. Aminuzzaman, M. Akhtaruzzaman, G. Muhammad, S. Ogawa, A. Watanabe, L.-H. Tey, Green Synthesis and Characterization of CuO Nanoparticles Derived from Papaya Peel Extract for the Photocatalytic Degradation of Palm Oil Mill Effluent (POME), Sustainability, 13 (2021) 796.

[21] K.P. Sapkota, I. Lee, M. Hanif, M. Islam, J. Akter, J.R. Hahn, Enhanced visible-light photocatalysis of nanocomposites of copper oxide and single-walled carbon nanotubes for the degradation of methylene blue, Catalysts, 10 (2020) 297.

[22] PRS Kodavanti, JE Royland, K.S. Rao, Toxicology of Persistent Organic Pollutants, in: Reference module in biomedical sciences, 2014.

[23] United States Environmental Protection Agency, Persistent Organic Pollutants: A Global Issue, A Global Response, in, US Environmental Protection Agency, Washingtom DC, USA, 2020.

[24] S.K. Sharma, Green Chemistry and Water Remediation: Research and Applications, Elsevier, 2020.

[25] R. Gupta, D. Archambeault, H.-C. Yao, Genetic Mouse Models for Female Reproductive Toxicology Studies, (2010).

[26] M.A. Sainio, Chapter 7 - Neurotoxicity of solvents, in: M. Lotti, M.L. Bleecker (Eds.) Handbook of Clinical Neurology, Elsevier, 2015, pp. 93-110.

[27] A.L. Srivastav, M. Ranjan, Chapter 1 - Inorganic water pollutants, in: P. Devi, P. Singh, S.K. Kansal (Eds.) Inorganic Pollutants in Water, Elsevier, 2020, pp. 1-15.

[28] EPAs List of Volatile Organic Compounds in order of toxicity, in, 2020.

[29] J.L. O'Donoghue, 69 - Organic Chemicals, in: S. Gilman (Ed.) Neurobiology of Disease, Academic Press, Burlington, 2007, pp. 745-758.

[30] A. Ajmal, I. Majeed, R.N. Malik, H. Idriss, M.A. Nadeem, Principles and mechanisms of photocatalytic dye degradation on TiO_2 based photocatalysts: a comparative overview, Rsc Advances, 4 (2014) 37003-37026.

[31] M. Pirilä, M. Saouabe, S. Ojala, B. Rathnayake, F. Drault, A. Valtanen, M. Huuhtanen, R. Brahmi, R.L. Keiski, Photocatalytic degradation of organic pollutants in wastewater, Topics in Catalysis, 58 (2015) 1085-1099.

[32] A. Bhattacharjee, M. Ahmaruzzaman, CuO nanostructures: facile synthesis and applications for enhanced photodegradation of organic compounds and reduction of p-nitrophenol from aqueous phase, RSC Advances, 6 (2016) 41348-41363.

[33] V.K. Mrunal, A.K. Vishnu, N. Momin, J. Manjanna, Cu_2O nanoparticles for adsorption and photocatalytic degradation of methylene blue dye from aqueous medium, Environmental Nanotechnology, Monitoring & Management, 12 (2019) 100265.

[34] M.P. Rao, J.J. Wu, A.M. Asiri, S. Anandan, Photocatalytic degradation of tartrazine dye using CuO straw-sheaf-like nanostructures, Water Science and Technology, 75 (2017) 1421-1430.

[35] S. Raha, D. Mohanta, M. Ahmaruzzaman, Novel $CuO/Mn_3O_4/ZnO$ nanocomposite with superior photocatalytic activity for removal of Rabeprazole from water, Scientific Reports, 11 (2021) 15187.

[36] N. D, K.K. Kondamareddy, H. Bin, D. Lu, P. Kumar, R.K. Dwivedi, V.O. Pelenovich, X.-Z. Zhao, W. Gao, D. Fu, Enhanced visible light photodegradation activity of RhB/MB from aqueous solution using nanosized novel Fe-Cd co-modified ZnO, Scientific Reports, 8 (2018) 10691.

[37] G.K. Weldegebrieal, H.H. Dube, A.K. Sibhatu, Photocatalytic activity of CdO/ZnO nanocomposite for methylene blue dye and parameters optimisation using response surface methodology, International Journal of Environmental Analytical Chemistry, (2021) 1-23.

[38] G.K. Weldegebrieal, A.K. Sibhatu, Photocatalytic activity of biosynthesized α-Fe_2O_3 nanoparticles for the degradation of methylene blue and methyl orange dyes, Optik, 241 (2021) 167226.

[39] M. Chauhan, N. Kaur, P. Bansal, R. Kumar, S. Srinivasan, G.R. Chaudhary, Proficient Photocatalytic and Sonocatalytic Degradation of Organic Pollutants Using CuO Nanoparticles, Journal of Nanomaterials, 2020 (2020) 6123178.

[40] S. Haseena, S. Shanavas, J. Duraimurugan, T. Ahamad, S.M. Alshehri, R. Acevedo, N. Jayamani, Investigation on photocatalytic and antibacterial ability of green treated copper oxide nanoparticles using Artabotrys Hexapetalus and Bambusa Vulgaris plant extract, Materials Research Express, 6 (2019) 125064.

[41] N. Dasineh Khiavi, R. Katal, S. Kholghi Eshkalak, S. Masudy-Panah, S. Ramakrishna, H. Jiangyong, Visible Light Driven Heterojunction Photocatalyst of CuO–Cu2O Thin Films for Photocatalytic Degradation of Organic Pollutants, Nanomaterials, 9 (2019) 1011.

[42] P. Raizada, A. Sudhaik, S. Patial, V. Hasija, A.A. Parwaz Khan, P. Singh, S. Gautam, M. Kaur, V.-H. Nguyen, Engineering nanostructures of CuO-based photocatalysts for water treatment: Current progress and future challenges, Arabian Journal of Chemistry, 13 (2020) 8424-8457.

[43] E.D. Revellame, D.L. Fortela, W. Sharp, R. Hernandez, M.E. Zappi, Adsorption kinetic modeling using pseudo-first order and pseudo-second order rate laws: A review, Cleaner Engineering and Technology, 1 (2020) 100032.

[44] F. Imtiaz, J. Rashid, M. Xu, Semiconductor Nanocomposites for Visible Light Photocatalysis of Water Pollutants, in: Concepts of Semiconductor Photocatalysis, IntechOpen, 2019.

[45] P. Mallick, S. Sahu, Structure, microstructure and optical absorption analysis of CuO nanoparticles synthesized by sol-gel route, Nanoscience and Nanotechnology, 2 (2012) 71-74.

[46] P. Nuengmatcha, P. Porrawatkul, S. Chanthai, P. Sricharoen, N. Limchoowong, Enhanced photocatalytic degradation of methylene blue using Fe_2O_3/graphene/CuO nanocomposites under visible light, Journal of Environmental Chemical Engineering, 7 (2019) 103438.

[47] A. Muthuvel, M. Jothibas, C. Manoharan, Synthesis of copper oxide nanoparticles by chemical and biogenic methods: photocatalytic degradation and in vitro antioxidant activity, Nanotechnology for Environmental Engineering, 5 (2020) 1-19.

[48] O.S. Junior, A. Monteiro, J. Oliveira, A. Araújo, D. Silva, J. Kulesza, B. Barros, Coordination polymer-derived CuO catalysts for oxidative degradation of methylene blue, Materials Chemistry and Physics, 235 (2019) 121737.

[49] A. Sadollahkhani, Z. Hussain Ibupoto, S. Elhag, O. Nur, M. Willander, Photocatalytic properties of different morphologies of CuO for the degradation of Congo red organic dye, Ceramics International, 40 (2014) 11311-11317.

[50] M. Nazim, A.A.P. Khan, A.M. Asiri, J.H. Kim, Exploring Rapid Photocatalytic Degradation of Organic Pollutants with Porous CuO Nanosheets: Synthesis, Dye Removal, and Kinetic Studies at Room Temperature, ACS Omega, 6 (2021) 2601-2612.

[51] L. Vimala Devi, S. Sellaiyan, T. Selvalakshmi, H.J. Zhang, A. Uedono, K. Sivaji, S. Sankar, Synthesis, defect characterization and photocatalytic degradation efficiency of Tb doped CuO nanoparticles, Advanced Powder Technology, 28 (2017) 3026-3038.

[52] R. Sasikala, K. Karthikeyan, D. Easwaramoorthy, I.M. Bilal, S.K. Rani, Photocatalytic degradation of trypan blue and methyl orange azo dyes by cerium loaded CuO nanoparticles, Environmental Nanotechnology, Monitoring & Management, 6 (2016) 45-53.

[53] R. Arunadevi, B. Kavitha, M. Rajarajan, A. Suganthi, A. Jeyamurugan, Investigation of the drastic improvement of photocatalytic degradation of Congo red by monoclinic Cd, Ba-CuO nanoparticles and its antimicrobial activities, Surfaces and Interfaces, 10 (2018) 32-44.

[54] A.M. El Sayed, M. Shaban, Structural, optical and photocatalytic properties of Fe and (Co, Fe) co-doped copper oxide spin coated films, Spectrochimica Acta Part A: Molecular and Biomolecular Spectroscopy, 149 (2015) 638-646.

[55] W.S. Koe, J.W. Lee, W.C. Chong, Y.L. Pang, L.C. Sim, An overview of photocatalytic degradation: photocatalysts, mechanisms, and development of photocatalytic membrane, Environmental Science and Pollution Research, 27 (2020) 2522-2565.

[56] K. Mageshwari, D. Nataraj, T. Pal, R. Sathyamoorthy, J. Park, Improved photocatalytic activity of ZnO coupled CuO nanocomposites synthesized by reflux condensation method, Journal of Alloys and Compounds, 625 (2015) 362-370.

[57] S.S. Hossain, M. Tarek, T.D. Munusamy, K.M.R. Karim, S.M. Roopan, S.M. Sarkar, C.K. Cheng, M.M.R. Khan, Facile synthesis of CuO/CdS heterostructure photocatalyst for the effective degradation of dye under visible light, Environmental Research, 188 (2020) 109803.

[58] S. Dursun, S.N. Koyuncu, İ.C. Kaya, G.G. Kaya, V. Kalem, H. Akyildiz, Production of CuO–WO_3 hybrids and their dye removal capacity/performance from wastewater by adsorption/photocatalysis, Journal of Water Process Engineering, 36 (2020) 101390.

[59] L. Wang, W. Si, Y. Tong, F. Hou, D. Pergolesi, J. Hou, T. Lippert, S.X. Dou, J. Liang, Graphitic carbon nitride (g-C_3N_4)-based nanosized heteroarrays: Promising materials for photoelectrochemical water splitting, Carbon Energy, 2 (2020) 223-250.

[60] G. Tzvetkov, J. Zaharieva, M. Tsvetkov, T. Spassov, A novel construction of Z-scheme CuO/g-C_3N_4 heterojunction for visible-light-driven photocatalysis in natural seawater, in:

International Conference on Quantum, Nonlinear, and Nanophotonics 2019 (ICQNN 2019), International Society for Optics and Photonics, 2019, pp. 113320B.

[61] N. Kumaresan, M.M.A. Sinthiya, K. Ramamurthi, R. Ramesh Babu, K. Sethuraman, Visible light driven photocatalytic activity of ZnO/CuO nanocomposites coupled with rGO heterostructures synthesized by solid-state method for RhB dye degradation, Arabian Journal of Chemistry, 13 (2020) 3910-3928.

[62] W. Bai, M. Wu, X. Du, W. Gong, Y. Ding, C. Song, L. Liu, Synergistic effect of multiple-phase rGO/CuO/Cu_2O heterostructures for boosting photocatalytic activity and durability, Applied Surface Science, 544 (2021) 148607.

[63] M.A. Bajiri, A. Hezam, K. Namratha, R. Viswanath, Q. Drmosh, H.B. Naik, K. Byrappa, CuO/ZnO/g-C_3N_4 heterostructures as efficient visible light-driven photocatalysts, Journal of Environmental Chemical Engineering, 7 (2019) 103412.

[64] S. Liu, J. Tian, L. Wang, Y. Luo, X. Sun, One-pot synthesis of CuO nanoflower-decorated reduced graphene oxide and its application to photocatalytic degradation of dyes, Catalysis Science & Technology, 2 (2012) 339-344.

[65] S.M. Botsa, K. Basavaiah, Removal of Nitrophenols from wastewater by monoclinic CuO/RGO nanocomposite, Nanotechnology for Environmental Engineering, 4 (2018) 1.

[66] S. Dutta, K. Das, K. Chakrabarti, D. Jana, S. De, S. De, Highly efficient photocatalytic activity of CuO quantum dot decorated rGO nanocomposites, Journal of Physics D: Applied Physics, 49 (2016) 315107.

[67] S. Sagadevan, J.A. Lett, G.K. Weldegebrieal, S. Garg, W.-C. Oh, N.A. Hamizi, M.R. Johan, Enhanced Photocatalytic Activity of rGO-CuO Nanocomposites for the Degradation of Organic Pollutants, Catalysts, 11 (2021) 1008.

[68] H. Koohestani, Photocatalytic performance of rod-shaped copper oxides prepared by spin coating, Micro & Nano Letters, 14 (2019) 339-343.

[69] G. Singh, S. Panday, M. Rawat, D. Kukkar, S. Basu, Facile synthesis of CuO semiconductor nanorods for time dependent study of dye degradation and bioremediation applications, in: Journal of Nano Research, Trans Tech Publ, 2017, pp. 154-164.

[70] J. Singh, V. Kumar, K.-H. Kim, M. Rawat, Biogenic synthesis of copper oxide nanoparticles using plant extract and its prodigious potential for photocatalytic degradation of dyes, Environmental Research, 177 (2019) 108569.

[71] R. Saravanan, S. Karthikeyan, V. Gupta, G. Sekaran, V. Narayanan, A. Stephen, Enhanced photocatalytic activity of ZnO/CuO nanocomposite for the degradation of textile dye on visible light illumination, Materials Science and Engineering: C, 33 (2013) 91-98.

[72] P. Yugandhar, T. Vasavi, B. Shanmugam, P.U.M. Devi, K.S. Reddy, N. Savithramma, Biofabrication, characterization and evaluation of photocatalytic dye degradation efficiency of Syzygium alternifolium leaf extract mediated copper oxide nanoparticles, Materials Research Express, 6 (2019) 065034.

[73] R. Katwal, H. Kaur, G. Sharma, M. Naushad, D. Pathania, Electrochemical synthesized copper oxide nanoparticles for enhanced photocatalytic and antimicrobial activity, Journal of Industrial and Engineering Chemistry, 31 (2015) 173-184.

[74] N. Mukwevho, E. Fosso-Kankeu, F. Waanders, N. Kumar, S.S. Ray, X.Y. Mbianda, Photocatalytic activity of $Gd_2O_2CO_3$ ZnO CuO nanocomposite used for the degradation of phenanthrene, SN Applied Sciences, 1 (2019) 1-11.

[75] S. Sonia, I. Jose Annsi, P. Suresh Kumar, D. Mangalaraj, C. Viswanathan, N. Ponpandian, Hydrothermal synthesis of novel Zn doped CuO nanoflowers as an efficient photodegradation material for textile dyes, Materials Letters, 144 (2015) 127-130.

[76] A.L.K. Venkata, S.P. Anthony, M.S. Muthuraman, Synthesis of Solanum nigrum mediated copper oxide nanoparticles and their photocatalytic dye degradation studies, Materials Research Express, 6 (2019) 125402.

[77] N. Akram, J. Guo, W. Ma, Y. Guo, A. Hassan, J. Wang, Synergistic catalysis of co $(oH)_2$/cuo for the Degradation of organic pollutant Under Visible Light irradiation, Scientific reports, 10 (2020) 1-12.

[78] M.K. Date, L.-H. Yang, T.-Y. Yang, K.-y. Wang, T.-Y. Su, D.-C. Wu, Y.-L. Cheuh, Three-dimensional CuO/TiO_2 hybrid nanorod arrays prepared by electrodeposition in AAO membranes as an excellent Fenton-like photocatalyst for dye degradation, Nanoscale research letters, 15 (2020) 1-12.

[79] K. Benabbas, N. Zabat, I. Hocini, Facile synthesis of Fe_3O_4/CuO a core-shell heterostructure for the enhancement of photocatalytic activity under visible light irradiation, Environmental Science and Pollution Research, 28 (2021) 4329-4341.

[80] A.A.M. Sakib, S.M. Masum, J. Hoinkis, R. Islam, M.A.I. Molla, Synthesis of CuO/ZnO Nanocomposites and Their Application in Photodegradation of Toxic Textile Dye, Journal of Composites Science, 3 (2019) 91.

[81] A.H. Abdullah, W.T. Peng, M. Hussein, Degradation of methylene blue dye by CuO-$BiVO_4$ photocatalysts under visible light irradiation, Malaysian Journal of Analytical Sciences, 20 (2016) 1338-1345.

[82] Z. Yang, Y. Yang, X. Zhu, G. Chen, W. Zhang, An outward coating route to CuO/MnO_2 nanorod array films and their efficient catalytic oxidation of acid fuchsin dye, Industrial & Engineering Chemistry Research, 53 (2014) 9608-9615.

[83] R.X. Chen, S.L. Zhu, J. Mao, Z.D. Cui, X.J. Yang, Y.Q. Liang, Z.Y. Li, Synthesis of CuO/Co_3O_4 Coaxial Heterostructures for Efficient and Recycling Photodegradation, International Journal of Photoenergy, 2015 (2015) 183468.

[84] R. Priya, S. Stanly, S.B. Dhanalekshmi, S. Sagadevan, Fabrication of photocatalyst MgO: CuO composite and enhancement of photocatalytic activity under UV light, Materials Research Express, 6 (2019) 125023.

[85] S. Sonia, I.J. Annsi, P.S. Kumar, D. Mangalaraj, C. Viswanathan, N. Ponpandian, Hydrothermal synthesis of novel Zn doped CuO nanoflowers as an efficient photodegradation material for textile dyes, Materials Letters, 144 (2015) 127-130.

[86] S. Iqbal, M. Javed, A. Bahadur, M.A. Qamar, M. Ahmad, M. Shoaib, M. Raheel, N. Ahmad, M.B. Akbar, H. Li, Controlled synthesis of Ag-doped CuO nanoparticles as a core with poly (acrylic acid) microgel shell for efficient removal of methylene blue under visible light, Journal of Materials Science: Materials in Electronics, 31 (2020) 8423-8435.

[87] E. Alp, H. Eşgin, M.K. Kazmanlı, A. Genc, Synergetic activity enhancement in 2D CuO-Fe_2O_3 nanocomposites for the photodegradation of rhodamine B, Ceramics International, 45 (2019) 9174-9178.

[88] S. Norzaee, B. Djahed, R. Khaksefidi, F.K. Mostafapour, Photocatalytic degradation of aniline in water using CuO nanoparticles, Journal of Water Supply: Research and Technology-Aqua, 66 (2017) 178-185.

[89] K.L. Wasewar, S. Singh, S.K. Kansal, Chapter 13 - Process intensification of treatment of inorganic water pollutants, in: P. Devi, P. Singh, S.K. Kansal (Eds.) Inorganic Pollutants in Water, Elsevier, 2020, pp. 245-271.

[90] G.K. Kinuthia, V. Ngure, D. Beti, R. Lugalia, A. Wangila, L. Kamau, Levels of heavy metals in wastewater and soil samples from open drainage channels in Nairobi, Kenya: community health implication, Scientific Reports, 10 (2020) 8434.

[91] A.T. Le, S.-Y. Pung, S. Sreekantan, A. Matsuda, D.P. Huynh, Mechanisms of removal of heavy metal ions by ZnO particles, Heliyon, 5 (2019) e01440.

[92] I.G. Wenten, K. Khoiruddin, A.K. Wardani, I.N. Widiasa, Chapter 5 - Synthetic polymer-based membranes for heavy metal removal, in: A.F. Ismail, W.N.W. Salleh, N. Yusof (Eds.) Synthetic Polymeric Membranes for Advanced Water Treatment, Gas Separation, and Energy Sustainability, Elsevier, 2020, pp. 71-101.

[93] G. Ren, H. Han, Y. Wang, S. Liu, J. Zhao, X. Meng, Z. Li, Recent Advances of Photocatalytic Application in Water Treatment: A Review, Nanomaterials, 11 (2021) 1804.

[94] A.T. Le, S.-Y. Pung, S. Sreekantan, A. Matsuda, D.P. Huynh, Mechanisms of removal of heavy metal ions by ZnO particles, Heliyon, 5 (2019) e01440-e01440.

[95] N. Wang, F. Zhang, Q. Mei, R. Wu, W. Wang, Photocatalytic TiO_2/rGO/CuO Composite for Wastewater Treatment of Cr(VI) Under Visible Light, Water, Air, & Soil Pollution, 231 (2020) 223.

[96] V.K. Sharma, M. Sohn, Aquatic arsenic: Toxicity, speciation, transformations, and remediation, Environment International, 35 (2009) 743-759.

[97] B. Nanda, A.C. Pradhan, K.M. Parida, Fabrication of mesoporous CuO/ZrO_2-MCM-41 nanocomposites for photocatalytic reduction of Cr(VI), Chemical Engineering Journal, 316 (2017) 1122-1135.

[98] Y. Li, C. Chen, Y. Wu, Y. Han, Y. Lan, Assessing the Photocatalytic Reduction of Cr(VI) by CuO in Combination with Different Organic Acids, Water, Air, & Soil Pollution, 228 (2017) 363.

[99] T.K. Tran, H.J. Leu, K.F. Chiu, C.Y. Lin, Electrochemical Treatment of Heavy Metal-containing Wastewater with the Removal of COD and Heavy Metal Ions, Journal of the Chinese Chemical Society, 64 (2017) 493-502.

[100] S.Z.N. Ahmad, W.N. Wan Salleh, A.F. Ismail, N. Yusof, M.Z. Mohd Yusop, F. Aziz, Adsorptive removal of heavy metal ions using graphene-based nanomaterials: Toxicity, roles of functional groups and mechanisms, Chemosphere, 248 (2020) 126008.

[101] A.R. Contreras Rodríguez, Removal of cadmium (II), lead (II) and chromium (VI) in water with nanomaterials, Universitat Autònoma de Barcelona, 2015.

[102] H.N. Muhammad Ekramul Mahmud, A. Huq, removal of heavy metal ions from wastewater/aqueous solution using polypyrrole-based adsorbents: a review, RSC advances, (2016).

[103] A. Saravanan, P.S. Kumar, M. Yashwanthraj, Sequestration of toxic Cr (VI) ions from industrial wastewater using waste biomass: A review, Desalination and Water Treatment, 68 (2017) 245-266.

[104] G.K. Kinuthia, V. Ngure, D. Beti, R. Lugalia, A. Wangila, L. Kamau, Levels of heavy metals in wastewater and soil samples from open drainage channels in Nairobi, Kenya: Community health implication, Scientific Reports, 10 (2020) 1-13.

[105] T. Sun, Z. Zhao, Z. Liang, J. Liu, W. Shi, F. Cui, Efficient As(III) removal by magnetic CuO-Fe_3O_4 nanoparticles through photo-oxidation and adsorption under light irradiation, Journal of Colloid and Interface Science, 495 (2017) 168-177.

[106] S.T. Ahamed, A. Ghosh, B. Show, A. Mondal, Fabrication of n-TiO_2/p-CuO thin-film heterojunction for efficient photocatalytic degradation of toxic organic dyes and reduction of metal ions in solution, Journal of Materials Science: Materials in Electronics, 31 (2020) 16616-16633.

[107] A.E. Nogueira, O.F. Lopes, A.B.S. Neto, C. Ribeiro, Enhanced Cr(VI) photoreduction in aqueous solution using Nb_2O_5/CuO heterostructures under UV and visible irradiation, Chemical Engineering Journal, 312 (2017) 220-227.

[108] J. Yu, S. Zhuang, X. Xu, W. Zhu, B. Feng, J. Hu, Photogenerated electron reservoir in hetero-p–n CuO–ZnO nanocomposite device for visible-light-driven photocatalytic reduction of aqueous Cr(vi), Journal of Materials Chemistry A, 3 (2015) 1199-1207.

[109] G. Nagaraju, One-pot synthesis of CueTiO_2/CuO nanocomposite: Application to photocatalysis for enhanced H2 production, dye degradation & detoxification of Cr (VI), international journal of hydrogen energy, 45 (2020) e7828.

[110] M.W. Kadi, R.M. Mohamed, A.A. Ismail, D.W. Bahnemann, Soft and hard templates assisted synthesis mesoporous CuO/g-C_3N_4 heterostructures for highly enhanced and accelerated Hg(II) photoreduction under visible light, Journal of Colloid and Interface Science, 580 (2020) 223-233.

[111] B. Prashanti, I. Sreevani, B. Suresh, T. Damodharam, Graphene-CuO nanocomposite for Efficient Photocatalytic Reduction of Pb (II) under Solar Light Irradiation, Applied Ecology and Environmental Sciences, 7 (2019) 176-181.

[112] R.M. Mohamed, A.A. Ismail, Photocatalytic reduction and removal of mercury ions over mesoporous CuO/ZnO S-scheme heterojunction photocatalyst, Ceramics International, 47 (2021) 9659-9667.

[113] Q. Xu, L. Zhang, B. Cheng, J. Fan, J. Yu, S-Scheme Heterojunction Photocatalyst, Chem, 6 (2020) 1543-1559